Exploring the Mechanical Properties of B_2O_3 Glass with Classical Molecular Dynamics Simulations

Master's thesis, 15.5.2024

Author:

Hanna Jääskö

Supervisor:

Janne Kalikka (Tampere University)
Pekka Koskinen

UNIVERSITY OF JYVÄSKYLÄ
DEPARTMENT OF PHYSICS

© 2024 Hanna Jääskö
This publication is copyrighted. You may download, display and print it for Your own personal use. Commercial use is prohibited. Julkaisu on tekijänoikeussäännösten alainen. Teosta voi lukea ja tulostaa henkilökohtaista käyttöä varten. Käyttö kaupallisiin tarkoituksiin on kielletty.

Abstract

Jääskö, Hanna
Exploring the Mechanical Properties of B_2O_3 Glass with Classical Molecular Dynamics Simulations
Master's thesis
Department of Physics, University of Jyväskylä, 2024, 59 pages

Inorganic oxide glasses have numerous applications, and they are used both in technology and industry. Inorganic oxide glasses are considered to be brittle, having little to no plastic deformation because of the amorphous structure of glass. Plasticity has been observed in aluminum oxide and densified silica, but little is known about the plasticity in boron oxide. Understanding the mechanical behavior of different oxide glasses can offer deeper insight into the applications of glasses.

In this master's thesis, the mechanical properties of boron oxide (B_2O_3) glass were studied with classical molecular dynamics simulations using LAMMPS. Here, it is shown that boron oxide can plastically deform up to 50% tensile strain at room temperature without a fracture. The mechanisms for the plasticity were analysed, and a significant amount of bond switching occurred during the simulation. The reason for this was found to be the improper three-dimensional structure that has weak van der Waals bonds holding the planar BO_3 building blocks together. This allowed for the deformation of the structure without a fracture. The plasticity occurred in small and random regions, and on average the deformation was quite minimal. Moreover, boron oxide exhibits larger elastic deformation compared to other oxide glasses due to its planar structure.

Keywords: Master's thesis, material physics, molecular dynamics, computational physics

Tiivistelmä

Jääskö, Hanna
B_2O_3-lasin mekaanisten ominaisuuksien tutkiminen klassisilla molekyylidynamiikkasimulaatioilla
Pro gradu-tutkielma
Fysiikan laitos, Jyväskylän yliopisto, 2024, 59 sivua.

Epäorgaanisilla laseilla on lukuisia käyttökohteita ja ne ovat tärkeitä teknologiassa ja teollisuudessa. Ne särkyvät helposti, eikä niillä esiinny plastista deformaatiota lasin amorfisen rakenteen vuoksi. Alumiinioksidissa sekä tihennetyssä piioksidissa on kuitenkin havaittu esiintyvän plastisuutta, mutta boorioksidin plastisuutta ei ole tutkittu. Eri oksidien mekaanisen käyttäytymisen ymmärtäminen voi tarjota syvemmän käsityksen lasien sovelluksista.

Tässä pro gradu-tutkielmassa tutkittiin boorioksidi (B_2O_3) lasin mekaanisia ominaisuuksia klassisilla molekyylidynamiikkasimulaatioilla käyttäen LAMMPS:ia. Tuloksena huomattiin, että boorioksidi pystyi venymään plastisesti jopa 50% huoneenlämmössä ilman murtumaa. Plastisuuden syitä tutkittiin ja merkittävä määrä sidosten vaihtumista huomattiin tapahtuneen simulaation aikana. Syy tälle on varsinaisen kolmiulotteisen rakenteen puuttuminen, minkä takia heikot van der Waals sidokset pitävät tasomaisia BO_3 rakennusosia kasassa. Tästä johtuen boorioksidi pystyi venymään plastisesti ilman murtumaa. Deformaatio tapahtui pienissä ja satunnaisissa alueissa ja oli keskimäärin melko pientä. Työssä huomattiin myös, että boorioksidilla oli suurempi elastinen venymä kuin muilla epäorgaanisilla laseilla, joka johtuu boorioksidin tasomaisesta rakenteesta.

Avainsanat: Pro gradu-tutkielma, materiaalifysiikka, molekyylidynamiikka, laskennallinen fysiikka

Preface

This master's thesis was done in the Materials and Molecular Modeling group of Tampere University. I am grateful for the opportunity to do my master's thesis on this topic. First, I would like to thank my supervisor Janne Kalikka for supervising this project and for all the advice and help throughout the process. I feel I learned a lot during this thesis process, especially about programming. I would also like to thank Pekka Koskinen for all the feedback and valuable corrections.

Lastly, I would like to thank all my friends, family, and Johannes for the support and encouragement during my studies.

Jyväskylä 14. May 2024

Hanna Jääskö

Contents

Abstract **3**

Tiivistelmä **5**

Preface **7**

1 Introduction **11**

2 Classical Molecular Dynamics Simulations **13**

2.1 The idea behind molecular dynamics 13

2.2 Ensembles 14

2.3 Force Field 15

2.4 Integrators 19

2.5 Periodic boundary conditions 20

2.6 Molecular dynamics simulation steps 22

3 Inorganic oxide glasses **25**

3.1 Glass structure and formation 25

3.2 Stress-strain behavior 28

3.3 Radial distribution function 32

4 Computational Methods **35**

4.1 Initial structure 35

4.2 Tensile simulations 37

5 Results **39**

5.1 Stress vs strain behavior 39

5.2 Radial distribution function 41

5.3 Coordination number analysis 42

5.4 Bond angle distribution 44

5.5 Non-affine squared displacement 45

5.6 Boroxol rings 46

6 Discussion **49**

7 Conclusions **53**

References **55**

A Radial distribution function 10 Å **59**

1 Introduction

Glass and its numerous unique properties have been a topic of interest since the discovery of glass making. The mechanical, optical, and chemical properties of glasses make them versatile and suitable for a variety of applications [1]. The uses of glass range from window panes to high-level nuclear waste disposal [2]. Glasses are used in electronics, healthcare, and as high-strength engineering materials [3, 4]. Most glasses in commercial use are silica-based, such as soda-lime-silica glass, which is used in glass panes and glass containers [1]. Besides silica based glasses, there are other glass forming materials, such as borate and phosphate glasses. Boron oxide is a significant component in borosilicate glasses, which are chemically durable and have good thermal shock resistance [3].

Typically, glasses are made by heating a glass forming material above its melting point, where it is then cooled down fast enough before the atoms settle for the typical ordered crystalline structure [5]. This way the disordered structure of glass is formed. The appearance of glass is solid-like but it has the atomic arrangement of a liquid. For this reason, the mechanical properties of glasses differ from those of crystalline solids. A key difference between crystalline solids and glass is the ability to deform plastically. Glasses are considered to deform only elastically until brittle failure [6]. This means that glasses do not typically deform plastically. The brittleness is caused by the amorphous structure of glass. In crystalline structures, such as metals, plastic deformation happens through dislocation planes slipping over each other. These dislocation planes are lines of defects in the crystal structure. Dislocation planes do not occur in glasses because the atomic arrangement in glasses is disordered. However, the plasticity mechanisms in glasses have been studied, and it has been found that plastic deformation can occur in glasses through bond switching [7]. The deformation does not occur by planes of atoms moving and gaining new neighboring atoms, it happens in smaller volumes, such as singular bonds breaking and then immediately forming new bonds. Plastic deformation in glasses, such as aluminum oxide and silica, has been studied experimentally and computationally [4, 8, 9]. It has been shown that contrary to the expected behavior of glasses, aluminum oxide can plastically deform via bond switching [4]. Moreover, densified silica in molecular dynamics simulations has also shown plastic deformation, although not as extensively as aluminum

oxide.

The complex nature of glass structure makes it a challenging task to model and study their behavior. Therefore, theoretical and computational methods are essential tools in understanding glass structure. One of these computational methods is molecular dynamics (MD) simulations. MD is a popular and widely used method to simulate large systems that can consist of millions of atoms [10]. In molecular dynamics, the classical equations of motion are solved numerically and as a result, a trajectory of the atoms' positions as a function of time is obtained. This way statistical information on the system's time evolution is known. The first molecular dynamics simulation was done in the 1950s and in 1976 the first MD simulation for oxide glass (silica) was performed [10, 11]. Since then, the interatomic potentials used in glasses have evolved tremendously and it is possible to obtain accurate knowledge on glasses.

The aim of this master's thesis was to study the mechanical properties of vitreous boron oxide when subjected to tensile strain. Especially whether boron oxide would exhibit plastic deformation, which has not been studied before. This was done with molecular dynamics simulations using LAMMPS, and the analysis was done with Ovito and with Fortran codes written as part of the thesis process. The structure of the thesis is as follows, first, the theory behind molecular dynamics is explained, followed by theory about glass structure and formation. After theory, the methods and simulation procedure are described and finally the results, discussion, and conclusions.

2 Classical Molecular Dynamics Simulations

This chapter explains the theory behind molecular dynamics. This includes description of force fields, ensembles, integrators, and periodic boundary conditions. In addition, common steps on performing a molecular dynamics simulation are presented.

2.1 The idea behind molecular dynamics

In classical molecular dynamics (MD) simulations, Newton's equations of motion are integrated for a system consisting of N particles and as a result, the time evolution of the system is obtained. Classical MD assumes that nuclear and electronic motions are separated, based on the Born-Oppenheimer approximation [12]. This makes it possible to run simulations for large systems containing millions of atoms since the energy of the system depends only on the nuclear coordinates. Given that the quantum mechanical properties of the molecules are not considered, the molecules are portrayed by a simple "ball and spring" model, which makes the calculations less time consuming [13]. While the separation of the nuclear and electronic motion makes the computational cost of MD less compared to other methods, it has its limitations. Moreover, the reliability of MD simulations depends heavily on the potential model used.

In order to perform a molecular dynamics simulation, a set of initial positions, and velocities, usually obtained from Maxwell distribution, as well as a representation of the forces between particles are needed [14]. Once these are known, the classical equation of motion can be solved

$$m_i \frac{d^2\mathbf{r}_i}{dt^2} = -\frac{\partial}{\partial \mathbf{r}_i} U(\mathbf{r}_1, \mathbf{r}_2, .., \mathbf{r}_N), \tag{1}$$

where $U(\mathbf{r}_1, \mathbf{r}_2, ..., \mathbf{r}_N)$ is the potential energy dependent on each individual particle [15]. When this is solved numerically in small time steps, a trajectory of the particles' coordinates as a function of time is obtained. From this trajectory, physical properties such as temperature and pressure can be determined. The simulation system needs to reach equilibrium before the averaged properties of the trajectory can be determined. The time in which equilibrium is reached varies for different systems. The results from MD

simulations can be compared to experimental results since the simulation setup resembles experimental setup [16].

2.2 Ensembles

Molecular dynamics simulations result in a time evolution of a system. However, the physical properties of interest are not taken as time averages, but as ensemble averages [10]. Each result from the integration of equation (1) creates a slightly different configuration of the system with different positions and velocities, which are called *ensembles*. The ensemble obtained from solving the classical equation of motion is called a *microcanonical ensemble* (NVE), having a constant number of particles (N), volume (V) and total energy (E) [14].

In experiments, a system with fixed energy is not possible. The energy of the system fluctuates and keeping it constant would be rather complicated, which is why the system is often simulated in the *canonical ensemble*. In canonical ensemble (NVT), the number of particles (N), volume (V), and temperature (T) are kept constant. In MD simulations, the NVT ensemble is obtained by coupling the system to a heat bath. The temperature of the system is gradually changed with a temperature controlling algorithm called thermostat [13]. Thermostat adjusts the average temperature of the system to meet the desired temperature. The purpose is not to fix the temperature to a certain value. The temperature of the system is determined from the average kinetic energy

$$\langle E_{\text{kin}} \rangle = \frac{1}{2}(3N_{\text{atoms}} - N_{\text{constraint}} k_B T), \tag{2}$$

where the number of constraints is often three [13]. Since the temperature is equal to the average kinetic energy, the temperature is controlled to meet the desired temperature by scaling the velocities [17]. One popular thermostat algorithm is the Nosé-Hoover thermostat, which is an extended version of the standard Hamiltonian. The algorithm considers the heat bath to be a direct part of the system by adding an artificial variable s to the standard Hamiltonian [18]

$$H_{\text{Nosé}} = \Phi(q) + \sum \frac{p^2}{2ms^2} + (X+1)k_B T \ln(s) + \frac{p_s^2}{2Q}, \tag{3}$$

where s is the time-scale parameter and p_s is the conjugate momentum of the variable s. X is the system's degree of freedom, $\sum \frac{p^2}{2m}$ is the kinetic energy term of the normal Hamiltonian and $\Phi(q)$ is the potential energy term [19]. Therefore, the heat bath is

controlled with the s and p_s variables. There are other thermostat algorithms and the main difference between them is the way the heat bath is considered.

In addition to the canonical ensemble, an *isothermal-isobaric* (NPT) ensemble is often used in MD simulations. In the NPT ensemble, the number of particles (N), pressure (P), and temperature (T) are kept constant. The system is coupled to a pressure bath, where the pressure is controlled with a barostat algorithm that adjusts the volume of the system [13]. On the contrary to thermostat algorithms, where velocities are scaled, in barostat algorithms the positions of the atoms are scaled [13]. With each time step, the coordinates and box size are rescaled to achieve the desired average pressure. The pressure for pairwise potentials is defined as

$$PV = N_{\text{atom}} k_B T + \frac{1}{3} \left\langle \sum_{i<j}^{N_{\text{atom}}} \mathbf{r}_{ij} \cdot \mathbf{f}_{ij} \right\rangle_M , \tag{4}$$

where $\mathbf{r}_{ij}$ is the position, $\mathbf{f}_{ij}$ is the force between interacting atoms i and j. It is common to simulate a system under both NVT and NPT ensembles in order for the simulated results to correspond with experimental conditions [15].

2.3 Force Field

Finding a suitable force field for a simulation system is a crucial part of molecular dynamic simulations. Force fields describe the interactions between and within the atoms. It determines how the coordinates of the atoms depend on the energy of the system [15]. There are multiple different types of force fields available, and with the right choice, the accuracy and physical meaningfulness of the simulations can be improved. The parameters for force fields are obtained through experimental methods or from quantum mechanical calculations [20]. Force fields are based on an assumption, in which the nuclear and electronic motions are separated because nuclei are significantly heavier than electrons. This enables the calculation of the system energy based on only the nuclear coordinates [12, 20]. Force fields aim to characterize quantum mechanical problems with classical mechanics [15]. Typically, a force field includes both intramolecular (bonded) and intermolecular (non-bonded) terms to describe the potential energy of the system

$$U = \sum U_{\text{bonded}} + \sum U_{\text{non-bonded}}. \tag{5}$$

This is the potential expressed in equation (1) and the key terms are illustrated in figure 1.

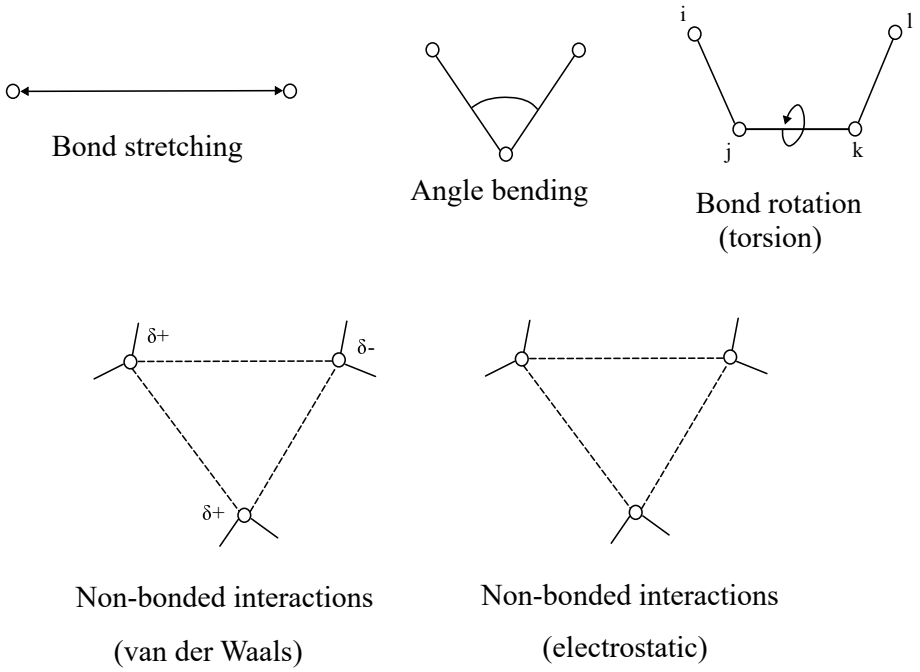

Figure 1. Descriptive figure of the intramolecular and intermolecular terms in force field. The figure is based on the book [12].

The bonded terms include bonds, angles as well as torsion and dihedral components [15]

$$U_{\text{bonded}} = \sum_{\text{bonds}} \frac{1}{2} k_b (r - r_0)^2 + \sum_{\text{angles}} \frac{1}{2} k_b (\theta - \theta_0)^2 + \sum_{\text{dihedrals}} \frac{V_n}{2} [1 + \cos(n\phi_{ijkl} - \delta)] + \sum_{\text{impropers}} \frac{k_{\text{imp}}}{2} [1 + \cos(2\omega_{ijkl} - \pi)]. \tag{6}$$

In equation (6) the first term is bond stretching, which represents the interactions between bonded atoms. Usually, it is modeled by harmonic potential, where r is the bond length, r_0 is the reference bond length, and k_b is the bond force constant. The second term is angle bending, which is also modeled by a harmonic potential, but in this case, it depends on the valence angles. The last two terms consist of two types of torsional potential: dihedral and improper dihedral energies. This potential represents the variation in energy related to the bond rotation, often expressed as a series expansion of the cosine function. The height of the potential barrier is V_n, n is the dihedral multiplicity, and δ is the phase factor. The torsional angle is ϕ_{ijkl}, which has four consecutive bonded atoms *i-j-k-l* involved, as can be seen in the figure 1. The last term is the improper dihedral

energy, which is used to preserve the planarity of specific atoms, and where k_{imp} is the force constant, and ω is the improper angle. [17]

The other part of the potential involves the intermolecular terms, or non-bonded terms, which concern the atoms in different molecules or atoms separated by 3 or more bonds [12]. They include a description for the van der Waals interactions, which model the attraction and repulsion between two atoms as well as for electrostatic interactions [15]. The van der Waals potential is most often expressed as the Lennard-Jones 12-6 potential

$$U_{\text{vdW}} = 4\epsilon \left[\left(\frac{\sigma_{ij}}{r_{ij}} \right)^{12} - \left(\frac{\sigma_{ij}}{r_{ij}} \right)^{6} \right], \tag{7}$$

where σ is the separation where the energy between two particles is zero, ϵ is the depth of the potential well, and r_{ij} is the distance between atoms i and j [12]. Even though this potential is the most popular, there are other potentials available if the Lennard-Jones potential is not suitable, for example, the Buckingham potential and the Beest Kramer van Santen (BKS) potential. These are used to model interactions between atoms that are not bonded. The Buckingham potential is

$$U_{\text{ij}} = A_{ij} e^{-r_{ij}/\rho_{ij}} - \frac{C_{ij}}{r_{ij}^6}, \tag{8}$$

where the constants A_{ij}, ρ_{ij} and C_{ij} are adjusted based on the atom types [17]. The Buckingham potential replaces the r^{12} term in the Lennard-Jones 12-6 potential with an exponential function, which is argued to be more accurate since the electron density as a function of distance is exponential [13]. However, the exponential term makes it computationally slower compared to the Lennard-Jones $12-6$ term. The BKS potential combines the Buckingham potential with a Coulomb force term

$$U_{\text{ij}} = \left(A_{ij} e^{-b_{ij} r_{ij}} - \frac{C_{ij}}{r_{ij}^6} \right) + \frac{q_i q_j}{r_{ij}}, \tag{9}$$

where A_{ij}, $b_{ij} = \frac{1}{\rho_{ij}}$ and C_{ij} are constants defined for different atom types [21]. The BKS potential is also called the Buckingham potential-incorporated Coulomb interaction. It was developed for complex systems involving silicas and aluminophosphates [2].

The other part of the intermolecular term is the electrostatic potential, which is calculated using Coulomb's law

$$U_{\text{Coul}} = \sum_{i=1}^{N_A} \sum_{j=1}^{N_B} \frac{q_i q_j}{4\pi\epsilon r_{ij}}, \tag{10}$$

where ϵ is the dielectric constant, r_{ij} is the distance between nuclei and q_i and q_j are the atomic charges. It is the sum of interaction between N_A and N_B, which are point charges [12].

2.4 Integrators

In order to solve the classical equation of motion (1) numerically, several different algorithms have been invented. Very straightforward way would be to use Taylor expansion for the positions of the particles $\mathbf{r}_i$ after a small time step $(t + \Delta t)$ [13]

$$\mathbf{r}_i(t + \Delta t) = \mathbf{r}_i(t) + \Delta t \frac{\mathrm{d}\mathbf{r}_i(t)}{\mathrm{d}t} + \frac{\Delta t^2}{2} \frac{\mathrm{d}\mathbf{r}_i(t)}{\mathrm{d}t} + \mathcal{O}(\Delta t^3). \tag{11}$$

Naturally, the positions of the particles before the current time can be obtained by changing the sign of the time step $(-\Delta t)$. Now, if the two versions of the Taylor expansion are summed, we get an expression for the next position of the particles

$$\mathbf{r}_i(t + \Delta t) \approx -\mathbf{r}_i(t - \Delta t) + 2\mathbf{r}_i(t) + \mathbf{a}_i(t)\Delta t^2 + \mathcal{O}(\Delta t^4), \tag{12}$$

which means that the next position of the particles after a small time step can be determined by only knowing the previous position, current position, and the acceleration $\mathbf{a}_i$ [14]. This is called the Verlet algorithm. A problem with this algorithm is the addition of large and small numbers together in the same equation, which can cause numerical inaccuracies. The truncation error is of order $\mathcal{O}(\Delta t^4)$ [17].

The Verlet algorithm does not solve velocities directly, but they can be calculated from

$$\mathbf{v}_i(t) = \frac{1}{2\Delta t}[\mathbf{r}_i(t + \Delta t) - \mathbf{r}_i(t - \Delta t)]. \tag{13}$$

However, velocities are calculated one time step later after the positions are calculated, so after $\mathbf{r}_i(t + \Delta t)$ has been calculated. This might cause problems with the accuracy of simulations that are done at constant temperature because the system's temperature is dependent on the kinetic energy [13].

Even though velocities are not necessary for solving the equation of motion, they can be used to calculate certain properties, such as kinetic energy. Therefore, a Velocity-Verlet algorithm, that includes velocities in addition to the positions, is often used. The Velocity-Verlet algorithm is [15]

$$\mathbf{r}_i(t + \Delta t) = \mathbf{r}_i(t) + \mathbf{v}_i(t)\Delta t + \frac{1}{2}\mathbf{a}_i(t)\Delta t^2, \tag{14}$$

$$\mathbf{v}_i(t + \Delta t) = \mathbf{v}_i(t) + \frac{1}{2}[\mathbf{a}_i(t) + \mathbf{a}_i(t + \Delta t)]\Delta t. \tag{15}$$

This way, the positions and velocities of each particle during every step of the simulation

are known. Velocity-Verlet calculates the positions and velocities at the same time step, not a one time step later like in the Verlet algorithm. The error term for Velocity-Verlet is $\mathcal{O}(\Delta t^2)$ [17] .

Another algorithm based on the Verlet algorithm is the Leapfrog algorithm [15]

$$\mathbf{r}_i(t + \Delta t) = \mathbf{r}_i(t) + \mathbf{v}_i(t + \frac{1}{2}\Delta t)\Delta t \tag{16}$$

$$\mathbf{v}_i(t + \frac{1}{2}\Delta t) = \mathbf{v}_i(t - \frac{1}{2}\Delta t) + \mathbf{a}_i(t)\Delta t. \tag{17}$$

The main difference compared to the original Verlet algorithm is the way velocities are determined. Velocities are calculated half a time step before the positions so that the velocities leap over the positions are calculated and then the positions leap over the velocities [13]. The numerical accuracy of the Leapfrog algorithm is better compared to the Verlet algorithm but the velocities are not calculated at the same time with the positions.

2.5 Periodic boundary conditions

One of the goals of MD simulations is to model and study macroscopic systems. However, simulating with a large number of atoms is computationally expensive. With periodic boundary conditions, it is possible to simulate smaller systems consisting of 10^3-10^4 atoms as if they were bulk material [12]. When simulating systems with a large number of atoms, the atoms near the edges of the simulation box would be in contact with a surface. Periodic boundary conditions are used to remove the surface effects and simulate large systems [22]. With this approach, a small part of the system called the unit cell is replicated in all directions and the atoms in each replicate have the same positions and velocities as in the original unit cell [14]. When an atom goes through the surface of the unit cell, it appears back to the cell from the opposite side. This is portrayed in the figure 2 as a two-dimensional example.

Periodic boundary conditions are considered when integrating the equations of motion. If an atom has moved outside of its cell, it needs to be wrapped back inside the cell [22]. This needs to be done after every step of the integration process. Periodic boundary conditions need to be also considered with atom interactions. Only the atoms that are within a certain cutoff distance of each other are assumed to interact with the nearest copy or image of the cell and therefore with the atoms near the opposite side, like in the figure 2 [14].

Furthermore, it is crucial to consider periodic boundary conditions during analysis to ensure realistic results.

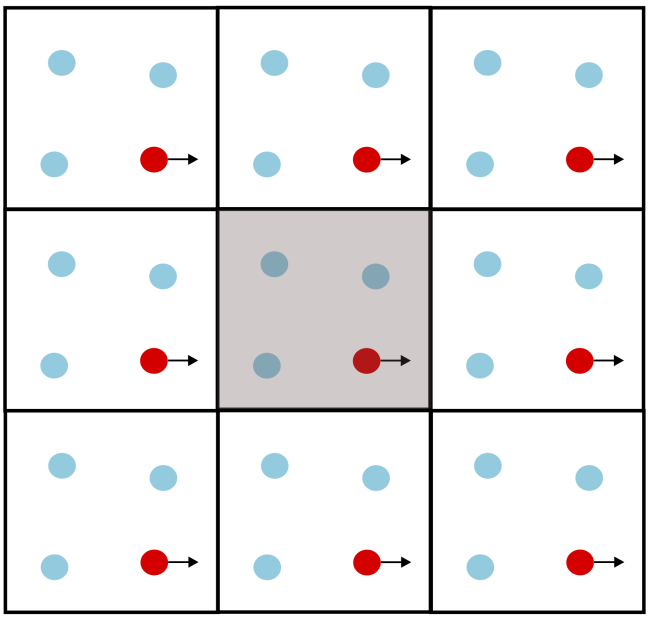

Figure 2. Periodic boundary conditions. There is only one original cell (the cell in the middle), the rest are just replicates of it with the same positions and velocities. The figure is based on reference [17].

2.6 Molecular dynamics simulation steps

The first step in performing a molecular dynamics simulation is setting up the system. First, the initial configuration of the system is created and a target density is set. The density of the system is controlled by changing the number of atoms and the simulation box dimensions. Additionally, this step includes selecting a suitable force field to describe the interactions between and within the molecules, choosing an integrator, and selecting the ensemble (NVE, NVT, NPT) in which the simulation is performed. [15]

Before starting the simulations, the system's energy needs to be minimized. In this stage, the energy is minimized by adjusting the arrangement of the coordinates. This ensures that the initial configuration of the atoms is proper, meaning that the system is in its most stable configuration. This also assures that there is no clashing between atoms. [12]

The third step is to simulate the system until equilibration is reached. In this step, the system is simulated at a desired temperature and/or pressure until it reaches equilibrium [15]. When simulating a system at a high temperature, it is possible to remove the long-range order of the structure. This is important when performing simulations in the liquid state since the initial structure is equivalent to a solid crystalline structure [12].

The final step consists of the actual production run, during which the system is allowed to evolve over a period of time. The forces are computed in small time steps, resulting in new positions and velocities of the atoms, which are then updated to a trajectory. An illustrative flow chart of the production run algorithm is shown in figure 3. During the simulation, important data is collected for further analysis. More often than not, the gathered data consist of thermodynamic properties, such as energy, temperature, and pressure. The simulation is typically carried out under NVT or NPT ensemble in order for the properties to be comparable with real experiments [16].

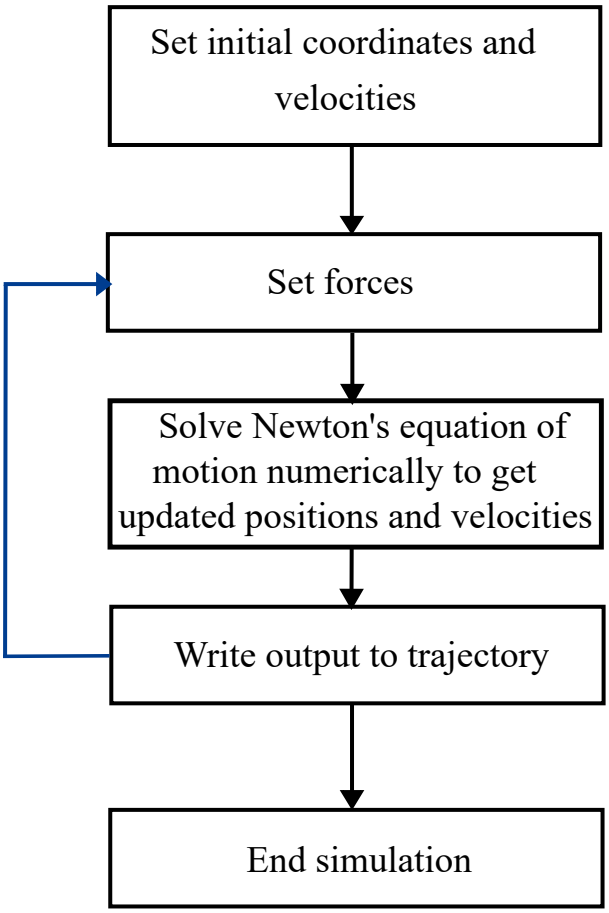

Figure 3. Different steps of the MD production run.

3 Inorganic oxide glasses

Inorganic oxide glasses are a common group of glasses, and the most popular glasses are silica (SiO_2) based, such as soda-lime-silica and borosilicate glass. However, there are also non-silica based glasses, such as alumina and boron oxide. In this chapter, the structure, formation, and properties of inorganic oxide glasses are explained. In addition, mechanical properties and behavior of materials, especially glasses, are explained. A common way to describe and model the mechanical behavior of materials involves stress and strain, especially focusing on the relationship between them. By inspecting the stress-strain curve of a material, different properties, such as elasticity, plasticity, and Young's modulus can be studied. Plasticity in glasses differs from crystalline materials, which is why both of them are discussed. In addition, the radial distribution function is explained because it is an important way to describe the structure of glass.

3.1 Glass structure and formation

Glass is a solid-like material that has the structure of a liquid [1]. Glasses are considered to be amorphous solids, which means that they do not have long-range periodic order. However, glasses have short-range and intermediate-range order, indicating some degree of order [3]. Moreover, glasses are also isotropic, meaning that they have the same properties and average packing in all three dimensions.

A common way to make glass is by first heating the material to a certain temperature (above the melting point), where it is held for a long enough time for the molecules to start vibrating around their lattice positions, and the crystal structure breaks. This way the long-range order of the structure is eliminated. Then it is rapidly cooled down to room temperature to avoid crystallization. This is illustrated in the $V - T$ diagram in figure 4 and the process results in supercooled liquid [3]. If the cooling is not fast enough, the material will crystallize, as shown in the $V - T$ diagram. As the cooling continues, the viscosity of the fluid increases, and therefore the motion of the atoms slows down and the formation of a crystal lattice is prevented [1]. Consequently, the atoms are unable to arrange themselves into the equilibrium configuration. The smooth curve after the

supercooled liquid state is called the glass transformation region, and within the region is a point where the extrapolated lines of glass and supercooled liquid cross, called the fictive temperature T_f [3]. The fictive temperature is different for each glass, and it means that the arrangement of atoms is similar as it would be in a liquid state. The transition from liquid to glass is not sharp like in crystalline materials. After the glass transition region, the material is considered to be glass and behaves like a solid [1]. In addition, from the $V - T$ diagram it can be seen that glasses have a larger volume than crystalline materials and therefore lower density. The fact that atoms in glasses are loosely packed causes differences in their structural properties compared to crystals, where the atoms are closely packed.

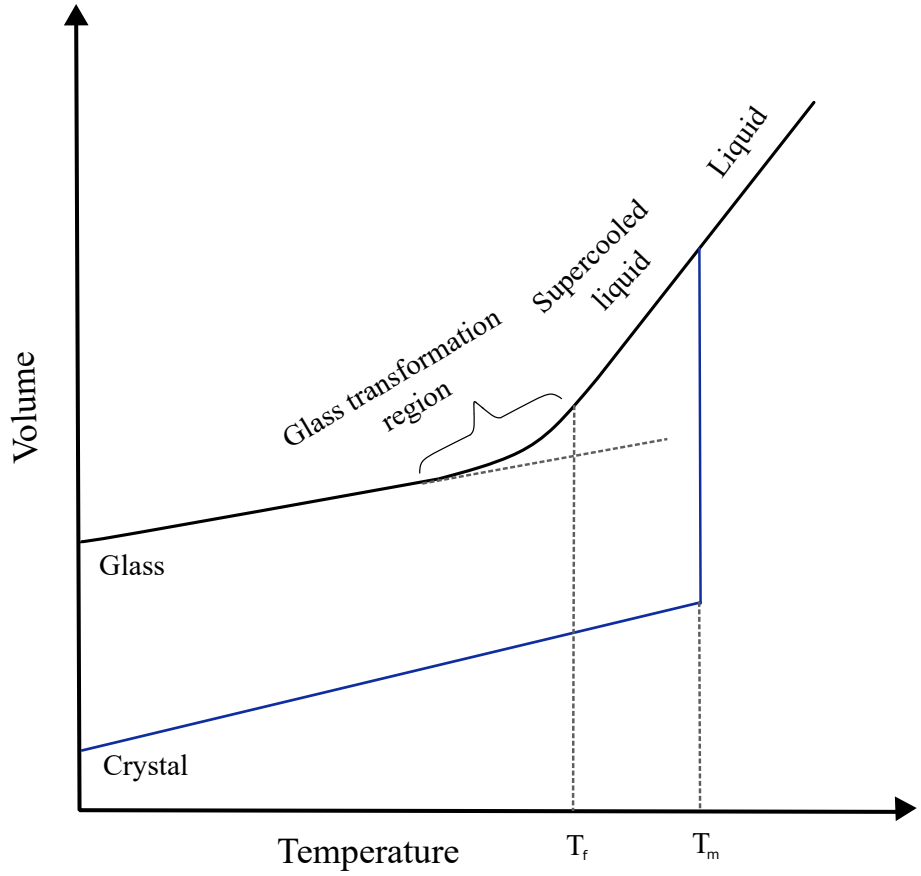

Figure 4. Volume-temperature diagram of glass forming. The liquid is heated above its melting temperature T_m, then rapidly cooled to prevent crystallization, resulting in the formation of a supercooled liquid. T_f is the fictive temperature and after the glass transformation region, the liquid is considered to be glass. [5]

While glasses do not have an ordered structure like crystals, they have a three-dimensional network structure, introduced by Zachariasen. The glass network theory is only applicable for oxide glasses and based on the criteria of the theory, it is possible to determine whether an oxide can form glass or not. The criteria for glass formation are (1) an oxygen atom is connected to a maximum of two cations, (2) the amount of oxygen atoms surrounding cations must be small, (3) oxygen polyhedra share corners rather than edges or faces, and (4) each oxygen polyhedron must share at least three corners. Every criterion must be filled in order for an oxide to form glass. However, rule 3 makes sure that the structure is open and random, which is crucial in the glass structure. Some oxides that fill these criteria and have been prepared in the glassy state are SiO_2, GeO_2, P_2O_5, and B_2O_3. [23]

Essentially, this theory proposes that glasses have short-range order and they have a three-dimensional network structure. An example of a glass structure, illustrating the lack of long-range order in glasses, is presented in figure 5. Furthermore, the figure demonstrates the change in bond angles and bond lengths between glass and crystal structures. The disorder in glasses comes from the varying lengths and angles of the bonds [1]. The glass network usually consists of tetrahedra or triangle-shaped *building blocks* that are connected by bridging and non-bridging bonds [3]. The shape of the building block is determined by the coordination number of the cation. For example, boron oxide (coordination number 3) has a triangular structure in a glassy state and the oxygen atoms form oxygen triangles that surround the boron atoms. Silica has a coordination number of 4 and therefore has a tetrahedral structure. Both boron oxide and silica are considered to be good network formers, which means that they can form glass by themselves. In addition to the criteria by Zachariasen, glass forming ability is considered to be dependent on the bond strength and bond types [1]. In the process of glass making, strong bonds restrict the atoms in the liquid state from returning back to the crystal structure. Purely ionic bonds are non-directional, which makes the formation of the glass network difficult. On the other hand, covalent bonds limit the bond angles to precise positions, which makes the network more periodic. Thus, good glass formers have bonds that are partially ionic and partially covalent [1].

Not all oxides can form glass by themselves. The type of oxides that cannot act as network formers are called modifiers. They can be added to glass to modify the network structure. For example, MgO, Na_2O, and Li_2O are modifiers. When a network modifier is added, the glass transformation temperature is lowered. In addition, some oxides can

act both as network formers and as network modifiers. These types of oxides are called intermediates, which include Al_2O_3 ZnO and PbO_2. [3]

In addition to short-range order, some glasses might also have intermediate range order [3]. The order can extend from the basic building blocks to a larger area. This explains the connection between the building blocks and whether they form rings or other intermediate units. For example, boron oxide shows sharp peaks in vibrational spectroscopic experiments, indicating a large fraction of boroxol rings [24].

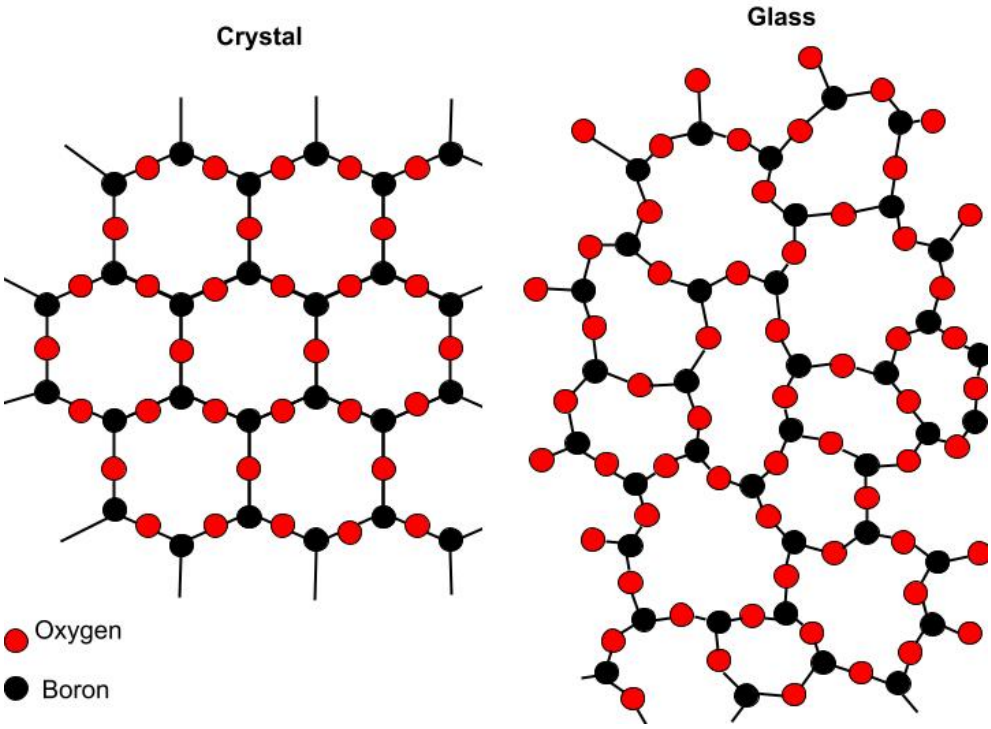

Figure 5. Two-dimensional example of the difference between crystal and glass structure. On the left is the crystal structure of solid boron oxide. On the right is the amorphous structure of boron oxide. [23]

3.2 Stress-strain behavior

Stress can be defined as the force acting on an object divided by its cross-sectional area

$$\sigma = \frac{F}{A}, \tag{18}$$

where σ is engineering stress, F is force and A is cross-sectional area. Stress causes an object to deform, and the deformation is measured by strain, which can be defined by the change in length divided by the original length

$$\epsilon = \frac{l - l_0}{l_0}, \tag{19}$$

where ϵ is engineering strain, l is the length of the material after stress is applied, and l_0 is the initial length. Therefore, strain measures the deformation of a material compared to its original size. [6]

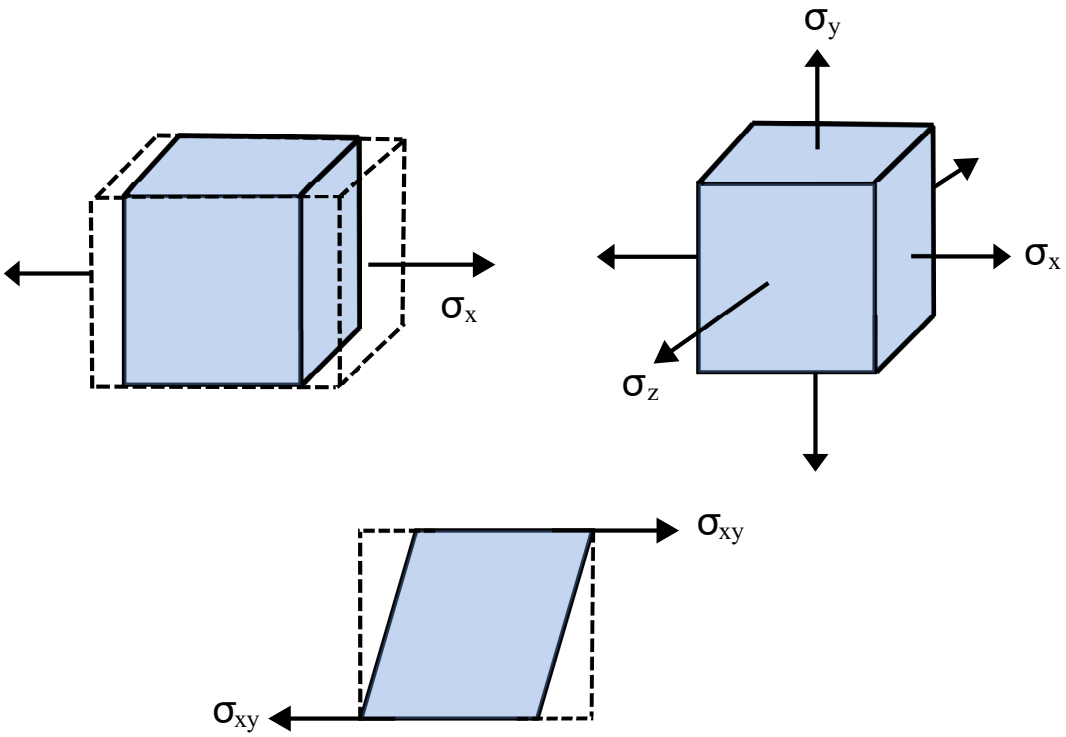

Figure 6. The box on the left is subjected to uniaxial stress and the box on the right is subjected to triaxial stress. The box on the bottom is subjected to shear stress. [1].

Three common types of stress are uniaxial stress, triaxial stress, and shear stress, and these can be seen in figure 6. Uniaxial stress can be tensile or compressive and it occurs only in one dimension σ_x, σ_y or σ_z. On the right in the figure 6 a rectangular box is subjected to triaxial stress σ_x, σ_y and σ_z in all three dimensions. An object can also be subjected to shear stress σ_{xy} if the force is parallel to the plane of the object. [1]

Observing the relationship between stress and strain provides information about the deformation of the material. In figure 7 is a stress-strain curve, where the linear part (A) in the beginning represents the elastic region of the material. Elasticity means that the material can return to its original size after stress is removed. When stress is applied to a material, the bonds between atoms stretch and bend but the deformation is not permanent [6].

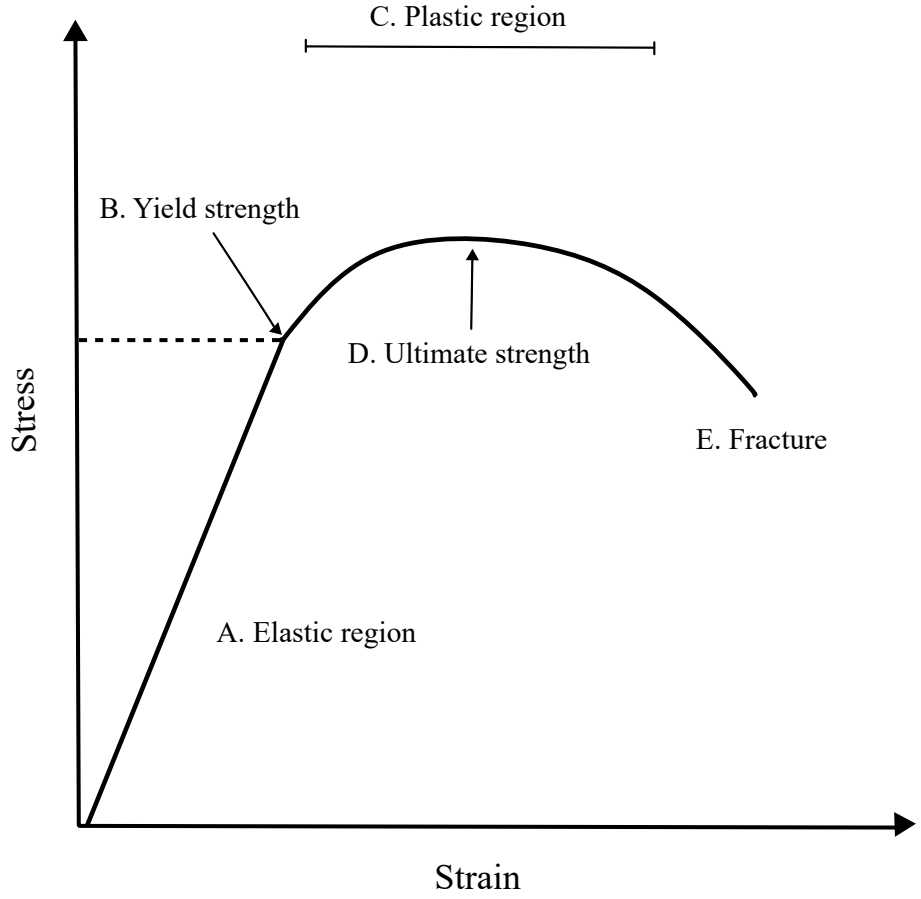

Figure 7. Stress strain curve of a ductile material. Elastic region (A), yield strength (B), plastic region (C), ultimate strength (D) and fracture (E).

The part in the stress-strain curve where the elastic region ends and plastic region starts (B), is called yield strength, which leaves a permanent strain of 0.002 when stress is removed. After this, plastic deformation starts (C). In the plastic region, the material undergoes irreversible deformation. This means that the atoms may gain new neighboring atoms and they settle in stable configuration with the new atoms around them [25]. Plastic deformation in solids happens through *slip*, which is caused by a defected plane/line of atoms, called *dislocations*, sliding over each other [26]. The plane containing dislocations is called the slip plane and the direction of the slip is the same as the direction of the dislocations [6]. In order for the slip planes to move, stress needs to be applied and the amount of stress depends on the crystal structure.

The larger the plastic region, the more ductile the material is. On the other hand, materials that are brittle exhibit hardly any plastic deformation [25]. Most ceramic materials, such as glasses, do not typically deform plastically, therefore they fracture

directly after the elastic deformation ends [1]. This is due to the strong ceramic/ionic bonds in glasses [7]. Moreover, glasses have small cracks and flaws on their surfaces, which also makes them brittle when stress is applied [25]. Stress is concentrated on the flaws, which then causes fracture. Because of the amorphous structure, glasses do not have similar dislocation planes as in crystalline structures. Therefore, the plasticity mechanism is different in amorphous materials compared to crystalline solids [1]. While glasses do not have dislocation planes, they have singular bonds that can break during the deformation process and then almost immediately form new bonds [7]. This phenomenon is called *bond switching*, during which atoms may also gain/lose neighboring atoms.

The maximum of the curve (D) is the ultimate strength or the tensile strength of the material. It is the maximum stress that the material can withstand. In other words, it describes how much the material can resist deformation. After the ultimate strength is reached, the cross-sectional area of the material starts to reduce. This is called necking which happens in ductile materials. After necking the material will fracture (E). [25]

Observing the stress-strain curve allows determination of various other properties, such as Young's modulus and Poisson's ratio. Young's modulus, also known as the elastic modulus, represents the ratio between tensile/compressive stress σ and tensile/compressive strain ϵ [6]. It is the slope of the linear part of the stress-strain curve in the figure 7. It is a measure of the strength of the material. The higher Young's modulus, the stronger the chemical bonds are [25]. For example, a diamond has Young's modulus of 1000 GPa, whereas for inorganic glasses it is $10 - 200$ GPa [3]. There are a few reasons why Young's modulus varies with different glasses. One is the glass transition temperature. The higher the glass transition temperature, the higher the Young's modulus [3]. Another reason is the amount of non-bridging oxygens in the glass structure. A high amount of non-bridging oxygens makes the glass network more disordered, making the structure prone to atom displacements and the material more ductile [3].

Poisson's ratio can be determined by dividing the lateral strain by the axial strain

$$\nu = -\frac{\epsilon_{\mathrm{l}}}{\epsilon_{\mathrm{a}}}, \tag{20}$$

where ϵ_{l} is the lateral strain and ϵ_{a} is the axial strain. Therefore Poisson's ratio represents the deformation in the lateral direction when tensile or compressive strain is applied. In rare cases, Poisson's ratio can be negative, which means that when the material is stretched, the cross-sectional area expands. For oxide glasses, the Poisson's ratio is often between 0.2 and 0.3. A higher Poisson's ratio means that the material has high elasticity

and does not fracture easily. [3]

3.3 Radial distribution function

The radial distribution function (RDF), sometimes called pair correlation function $g(r)$, is a useful way to obtain structural information on amorphous materials due to their lack of long-range order [22]. The radial distribution function is the probability of finding a particle at a distance r from another particle. This way average distances and arrangements of the atoms can be determined in disordered systems. RDF can be measured experimentally through x-ray diffraction and the results can be compared to simulated results [14]. The radial distribution function is determined as the following

$$g(r) = \rho^{-2}\left\langle \sum_i \sum_{j \neq i} \delta(r_i)\delta(r_j - r) \right\rangle = \frac{V}{N^2}\left\langle \sum_i \sum_{j \neq i} \delta(r - r_{ij}) \right\rangle \tag{21}$$

where ρ is the density, N is the total number of atoms, V is the volume of the spherical shell and δ is Dirac delta [2]. The radial distribution function can be calculated for the whole system or element wise. This way the pairwise distance between different elements can be determined.

Considering the scenario in figure 8 (a), the reference atom in the center has a spherical shell around it, with a distance r to another atom and width (Δr) and the volume of the shell is $4\pi r^2 \Delta r$. The number of atoms within the sphere is $4\pi r^2 \rho g(r)$ [10]. By integrating this between the lower and upper limits of r, the number of neighbors for an atom is obtained. This way the coordination number can be determined.

The atoms within the first sphere correspond to the first peak in figure 8 (b). These atoms are the nearest neighbors of the reference atom and the second peak corresponds to the second sphere. The first peak is the sharpest, and the number of atoms found in the other spheres decreases as the distance r increases. At larger distances, $g(r) \longrightarrow 1$ because glasses do not have long-range order, and $g(r) = 0$ at short distances because of the strong repulsive forces between atoms. The peaks do not have precise intervals as in crystalline solids because the atoms are loosely packed in glasses. The radial distribution function of glass resembles the structure of a liquid. [1]

Computationally RDF is determined by first calculating the pair-wise distances between all atoms. Only the distances that are within a specified cutoff distance, usually half of the box length, are considered. At larger distances, there are no interactions between atoms, and problems with periodic images might come up [22]. Then, the number of distances

that are between r and $r + \Delta r$ are stored. From these values, a histogram is made as a function of distance, and the values are normalized with the volume of the spherical shell and density. Normalization assures that with large distances $g(r) \longrightarrow 1$.

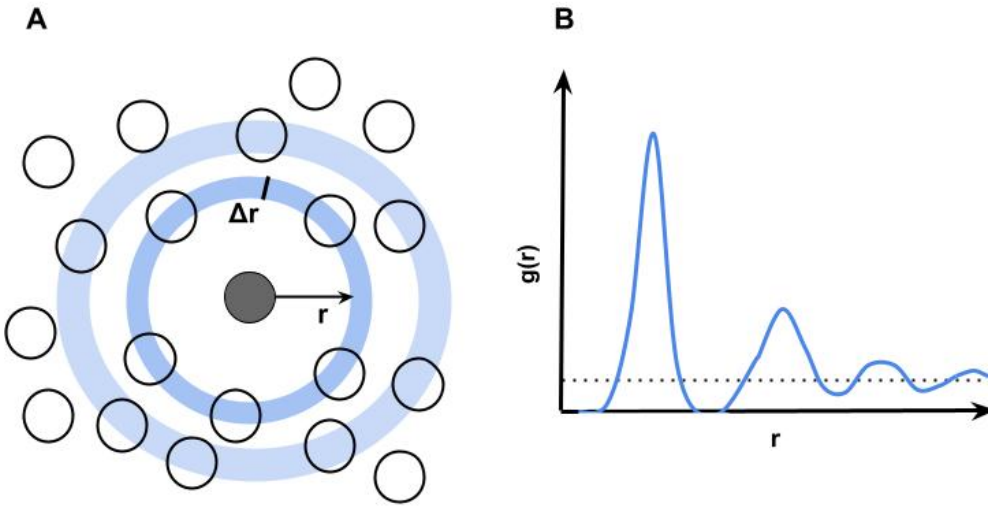

Figure 8. Descriptive figure of the radial distribution function. (**A**) atoms inside the first blues sphere correspond to the first peak of the radial distribution function in (**B**).

4 Computational Methods

In this chapter, the creation of the initial simulation structure as well as the simulations are explained. All MD simulations were performed on CSC – IT Center for Science supercomputer Mahti. Mahti has 1404 CPU nodes and 24 GPU nodes available, and these simulations were performed with 20 nodes and using all 128 cores in the node. The molecular dynamics simulations were performed with a Large-scale Atomistic/Molecular Parallel Simulator (LAMMPS), which is a classical molecular dynamics simulation code with a focus on material modeling [27]. LAMMPS is written in C++ and is designed to run on parallel machines.

4.1 Initial structure

In all of the simulations, the Nosé-Hoover thermostat and barostat were used when needed. Periodic boundary conditions are used throughout the simulations. The timestep for every simulation step was 1 fs and the Velocity-Verlet algorithm was used. The potential used was the BKS potential, which is the Buckingham potential with a Coulomb force term. The parameters of the BKS potential are shown in table 1 and the parameters A, ρ and C determine the narrowness of the potential [2].

Table 1. Van Beest, Kramer and van Santen (BKS) potential parameters for boron (B) and oxygen (O) [2].

pair	A(kcal/mol)	ρ (Å)	C (kcal Å^6 mol $^{-1}$)
B-B	2785.3	0.35	0.0
B-O	101323.7	0.17	0.0
O-O	207621.69	0.265	1955.7383

The amorphous boron oxide structure was prepared with a rectangular lattice with lattice vectors $a = 4.760200$, $b = 8.244908$, and $c = 12.993300$. The generated structure consisted of 1319760 atoms, with the lattice vectors repeated in all three dimensions, forming a simulation box with equal lengths of $L_x = L_y = L_z = 25$ nm. Energy minimization was performed on the system with the steepest descent algorithm. This ensured that the system's configurations were in a local potential energy minimum and prevented the overlapping of atoms.

Initially, the structure was in a crystalline form. Therefore, the structure was simulated at 3000 K in NVT ensemble, where it was equilibrated for 200 ps in order to eliminate the periodicity of the glass structure. After the structure was equilibrated at 3000 K, it was cooled down to 2000 K in NVT ensemble within 200 ps. The structure was then cooled further down to 1000 K in the NVT ensemble. At a temperature of 1000 K, the structure was equilibrated for 200 ps in NPT ensemble by coupling a Nosé-Hoover barostat to the system. This was done to control the pressure of the system. Then, the temperature was lowered to 300 K over a timespan of 1 ns in the NPT ensemble. With the used timestep and cooling time, the cooling rate was 5 K/ps. At 300 K the system was equilibrated at 1 atm pressure for an additional 200 ps. At a temperature of 300 K, the box lengths had expanded to 26 nm in each direction and the density was 1.73 g/cm^3. This way the structure was in amorphous form at room temperature. In figure 9 is the initial structure in amorphous form and also a closer view of the atomic arrangement of vitreous boron oxide.

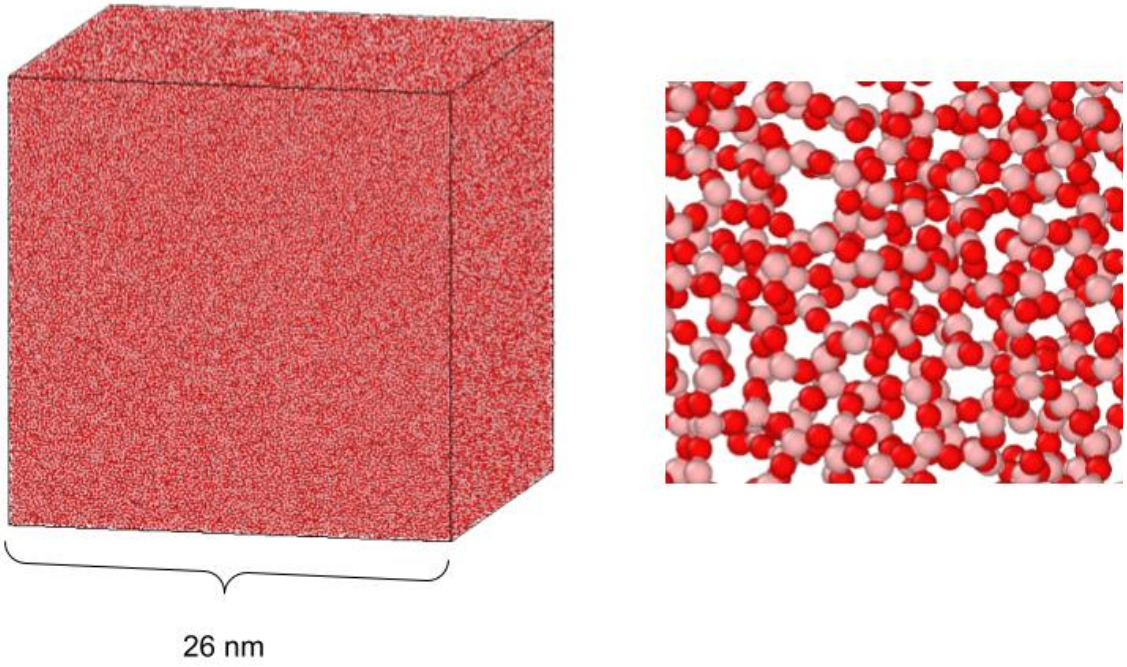

Figure 9. On the left is the initial simulation box of boron oxide at 300 K in amorphous form and on the right is a closer image of the atomic structure.

4.2 Tensile simulations

In the next phase, a tensile stress was applied separately to each dimension of the simulation box. Each result of the tensile simulation is slightly different due to the amorphous structure of glass. Therefore, the results are averaged to obtain more reliable information on the deformation.

The initial cubic box had a length of 26 nm on each side. The temperature was kept at 300 K and uniaxial stress was applied to one side, while the other two were kept at 1 atm pressure with a barostat. This was repeated for x, y, and z directions separately, so in total three different tensile simulations were performed. In LAMMPS, tensile deformation is achieved by adjusting the size of the box with each timestep. The engineering rate is defined as the velocity over the initial length. With the original box length set to 260 Å, a 50% tensile strain over a timespan of 1 ns corresponds to a rate of change of 0.000130 Å/fs. This rate of change represents the rate at which the length of the simulation box deforms,

resulting in an engineering strain rate of 0.5×10^9 1/s. Figure 10 shows the simulation box before and after the deformation. At the end, the strained side had a length of 39 nm, while the other two sides were approximately 21.7 nm long.

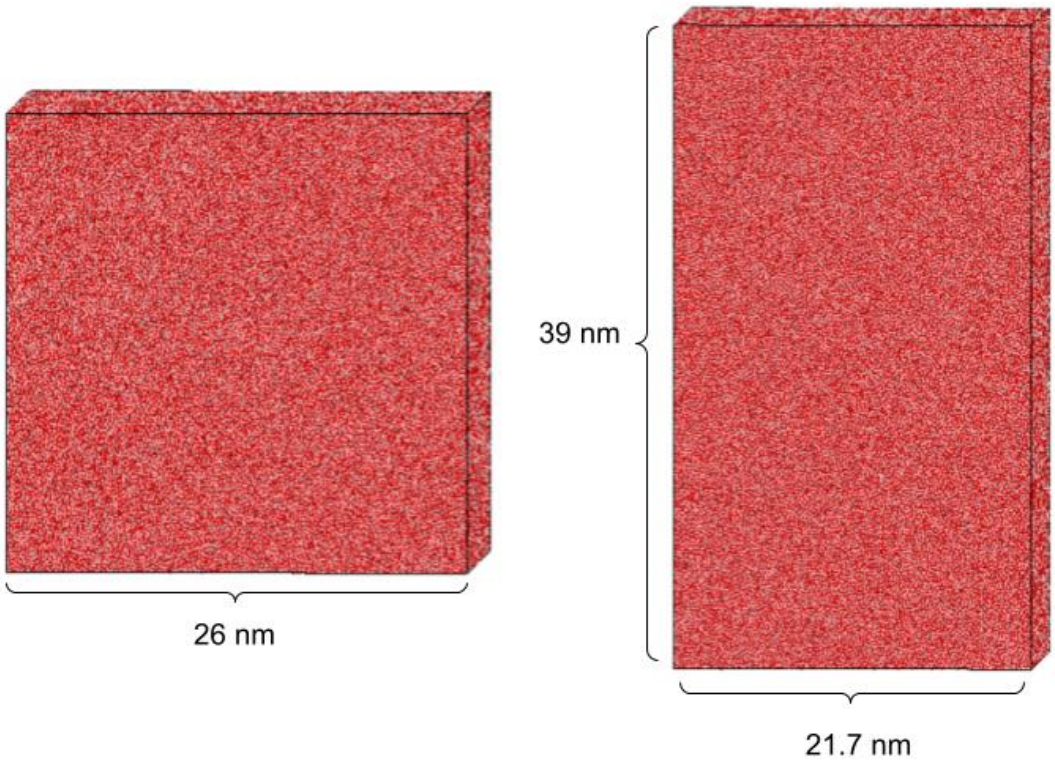

Figure 10. On the left is the cubic simulation box with all lengths equal to 26 nm. On the right is the simulation box after the 50% tensile strain (in the z-direction). The side that had been subjected to tensile stress had a length of 39 nm and the other two sides had a length of approximately 21.7 nm.

5 Results

In this chapter the results from the molecular dynamics simulations are presented. Data visualization and analysis tool Ovito was used to calculate the radial distribution function and non-affine squared displacement D^2_{min}. Results for the stress-strain curve, evolution of the coordination number, and bond angle distribution are also presented.

5.1 Stress vs strain behavior

The stress-strain curve of all three simulations is in figure 11.

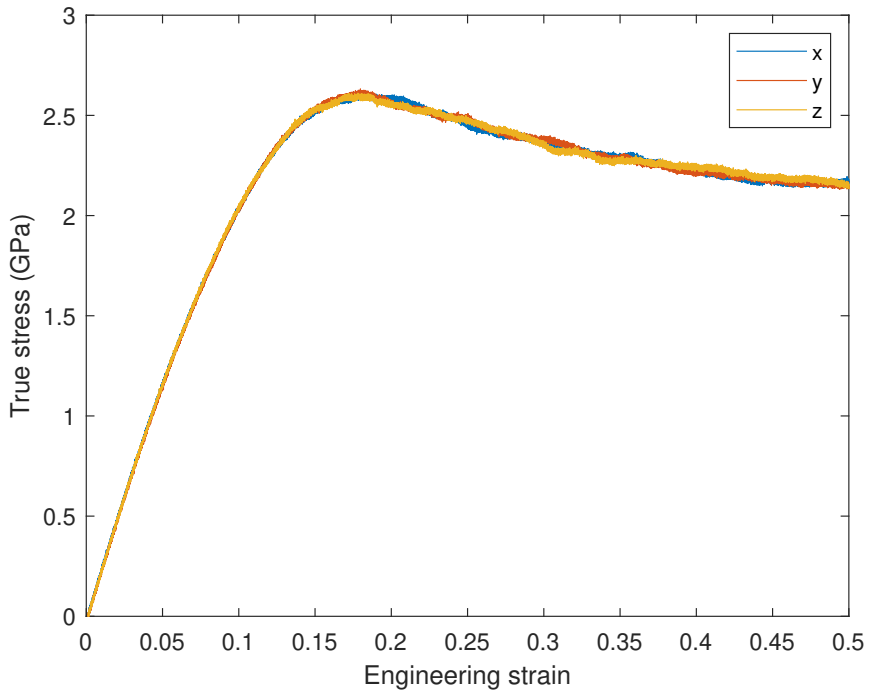

Figure 11. Stress strain curve of all three tensile test simulations. B_2O_3 deforms elastically up to approximately $8 - 10\%$, ultimate stress is at 2.6 GPa.

The linear part is the elastic region, and the slope is 25.3 GPa, which is the Young's modulus. The ultimate strength is the highest point of the curve, which is 2.6 GPa and it occurs when the structure has deformed approximately 18%. The curve shows that boron

oxide has plasticity in the tensile tests, and no fracture in any of the three simulations. Poisson's ratio was determined from the tensile deformation, which was 0.33 and falls into the typical range for oxide glasses, although it is at the upper end of that range.

The density change during the tensile strain is in figure 12. It can be seen, that the change in density corresponds to the part in the stress-strain curve, where plastic deformation is considered to begin.

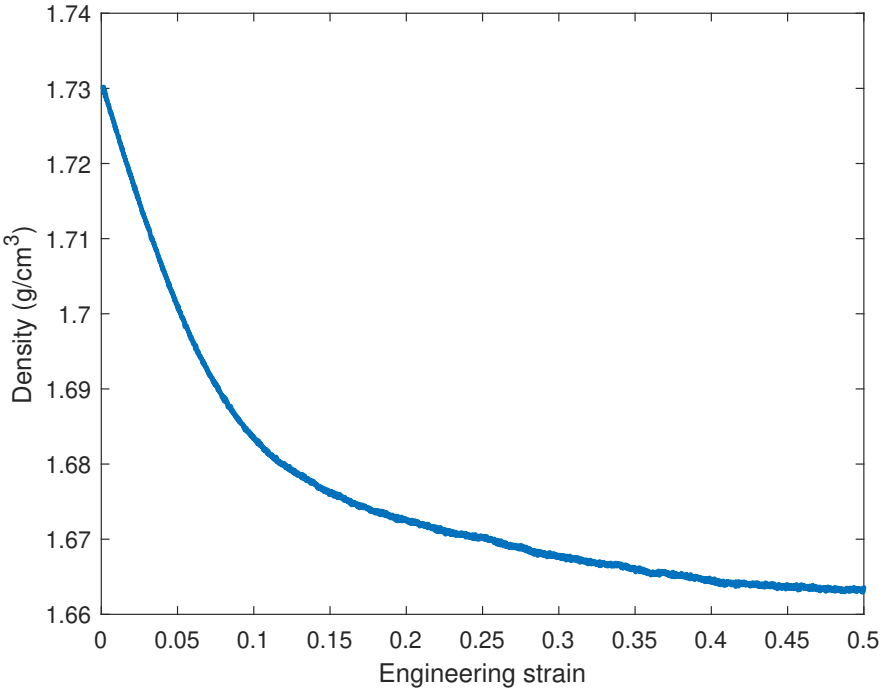

Figure 12. Average density as a function of strain.

5.2 Radial distribution function

The radial distribution function was calculated with Ovito [28]. Useful information on the deformation of the system can be obtained when inspecting the beginning of the simulation and the end of the simulation. The radial distribution function is presented in figure 13, which includes the average of three tensile simulations at the beginning and end of the tensile simulation. As seen in the figure, the structure of boron oxide remains approximately the same at the beginning and end of the deformation.

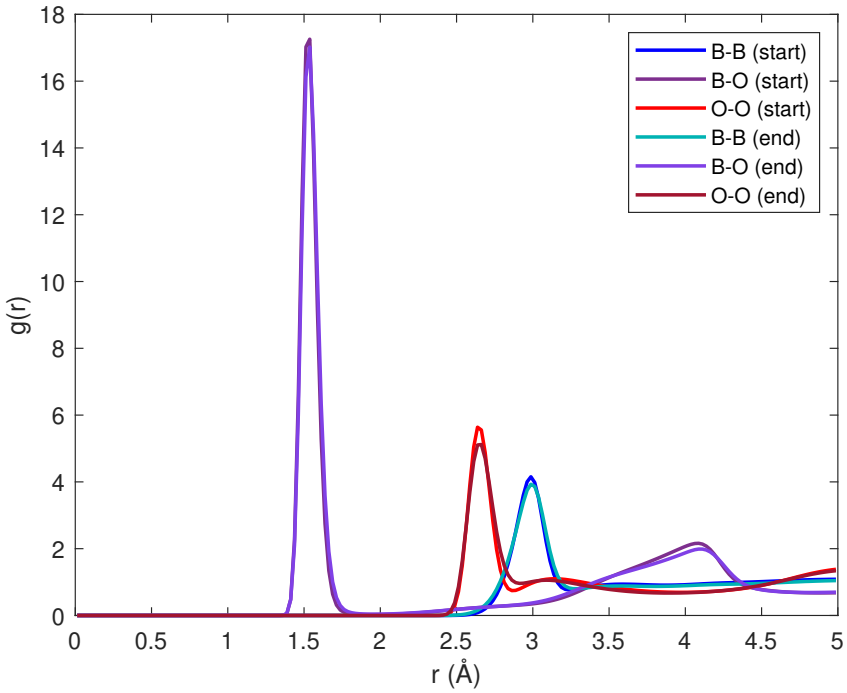

Figure 13. Radial distribution function. First and last 6% of the data are plotted. No noticeable difference in the structure between the start and end of the simulation.

There are no notable shifts in any of the peaks. The results show that the first peak (B-O) is at 1.53 Å and the first B-B peak is at 2.98 Å and the first O-O peak is at 2.63 Å. There is one other distinct peak for B-O at 4.13 Å. The cut-off radius was then determined to be 1.9 Å from the first minimum of the B-O $g(r)$. This means, that all atoms that were within 1.9 Å from each other were considered bonded, and therefore neighboring atoms. The peaks for O-O and B-B bonds are clearly separated from the B-O peak, which is why the cutoff of 1.9 Å can be used for all bonded atoms. At larger distances $g(r) \longrightarrow 1$, which is why the relevant part in terms of analysis is up to 5 Å. In Appendix A is the radial distribution function up to 10 Å.

5.3 Coordination number analysis

Coordination number (CN) was calculated for each tensile simulation using the cut-off radius determined from the radial distribution function. For this, all pairwise distances between atoms were calculated with a Fortran code, and if the distance between two atoms was within 1.9 Å, they were considered neighboring atoms. Periodic boundary conditions were considered in the calculations. Moreover, information about each atom's neighbors was collected for further analysis, meaning that the atom ID of every neighboring atom was saved. The evolution of the coordination number was analysed throughout each tensile simulation and was divided into four categories; increased CN, decreased CN, unchanged CN with the same neighboring atoms, and unchanged CN but at least one of the neighboring atoms changed.

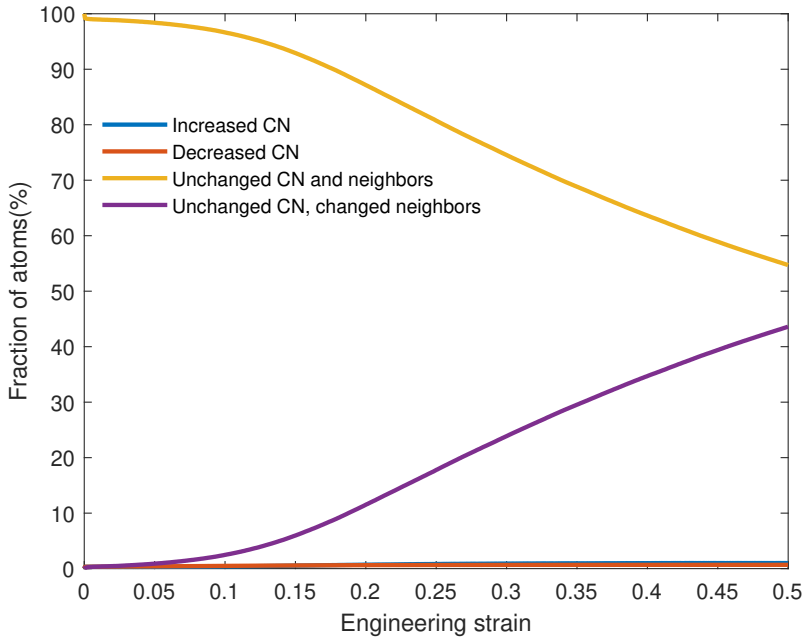

Figure 14. Coordination number (CN) analysis. The fraction of increased/decreased coordination numbers is less than 1%, the fraction of unchanged CN and neighbors is 55%, and the fraction of unchanged CN with at least one new neighboring atom is 44%.

The change in the coordination number is in figure 14 and it shows that the fraction of increased coordination number was 0.25% and the fraction of decreased coordination number was 0.7%. This means that throughout the tensile simulation, each atom had approximately the same number of neighboring atoms. At the end of the simulation, approximately 55% of the atoms had unchanged coordination numbers and the same neighbors, and 44% had unchanged coordination numbers but different neighboring atoms.

Further analysis with the coordination numbers was carried out, this time by tracking the most common coordination numbers for boron and oxygen, which were 3-coordinated for boron and 2-coordinated for oxygen. In figure 15 it can be seen that the fraction of 3-coordinated boron and 2-coordinated oxygen atoms are approximately 99% of the respective boron and oxygen atoms. A slight change (0.5%) in the coordination number of both boron and oxygen occurs as the tensile strain progresses. Furthermore, the fraction of 2-coordinated boron and 3-coordinated oxygen atoms were also calculated and can also be seen in the same figure, and the amounts were 0.25% and 0.7% respectively. In addition, 4-coordinated boron and oxygen atoms were also calculated, but the amounts were zero, which was expected from the high amount of 3-coordinated and 2-coordinated boron and oxygen atoms.

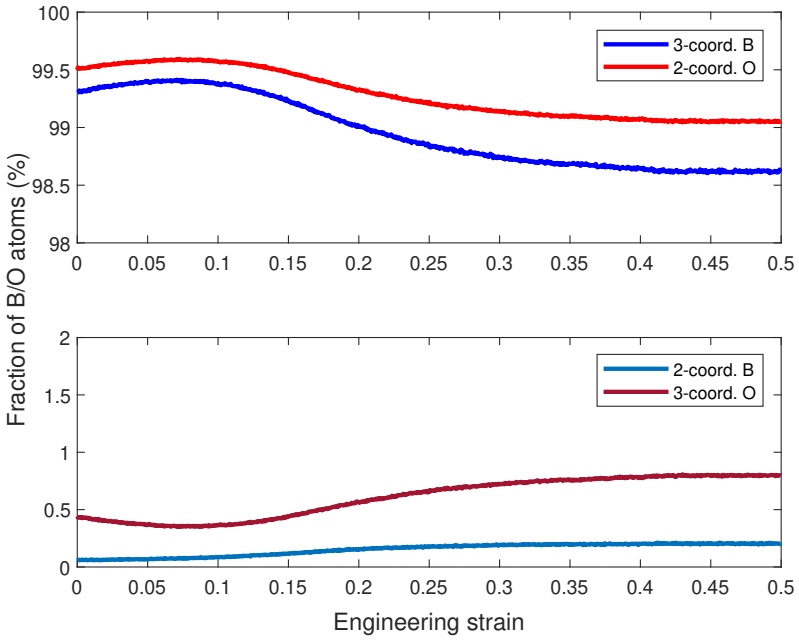

Figure 15. The evolution of 3-coordinated and 2-coordinated boron atoms and 2-coordinated and 3-coordinated oxygen atoms during the tensile simulation.

5.4 Bond angle distribution

The bond angle distribution was calculated with a Fortran code and the distributions of the O-B-O and B-O-B bonds are shown in figure 16. O-B-O bond angle distribution has a sharp peak at 120°, which comes from the planar structure of boron oxide. There are no other peaks in the O-B-O distribution. B-O-B bond angle has a wide peak at 155°, indicating a more fluctuating bond angle distribution.

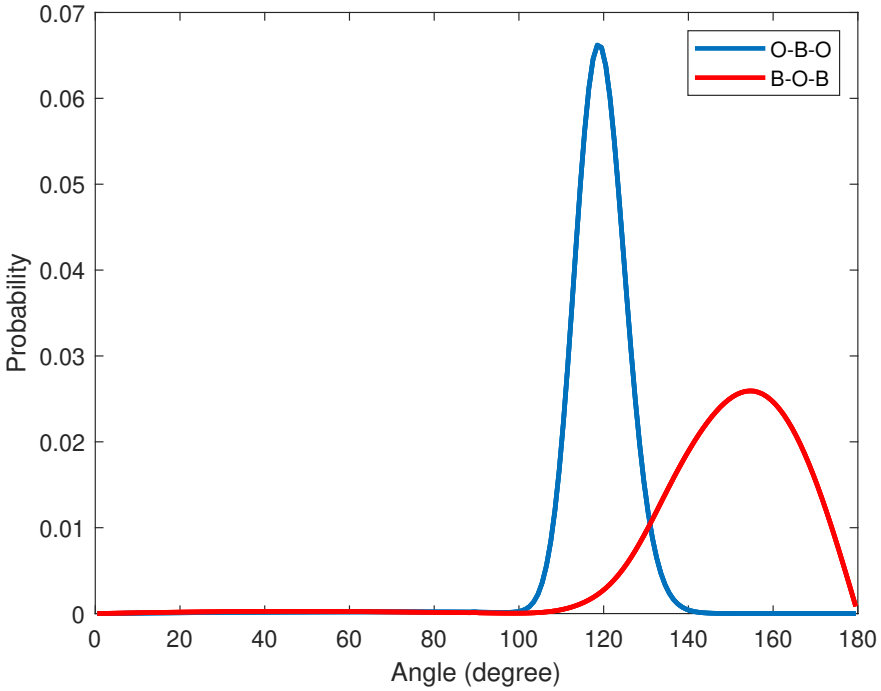

Figure 16. Averaged bond angle distribution for the O-B-O and B-O-B bond angle distributions from all three tensile simulations. O-B-O angle has a peak at 120° and B-O-B has a peak at 155°. The O-B-O peak is sharper than the B-O-B peak.

5.5 Non-affine squared displacement

Plasticity in amorphous materials occurs in smaller regions and can be determined and visualized by calculating the non-affine squared displacement (D^2_{min}) by Falk & Langer [29]. D^2_{min} was calculated with Ovito, and the periodic boundary conditions are considered by using an extended XYZ file. This way the changes in the box lengths were also taken into account. The cutoff radius for D^2_{min} is supposed to be 2.5 times the first maximum of $g(r)$, so in this case it was 3.8 Å. The reference configuration is the first frame, meaning that the cumulative D^2_{min} is calculated and visualized. In figure 17 the red areas are the atoms that have below average D^2_{min} and the blue areas have above average D^2_{min}. This means that the red areas have experienced minimal plasticity and the blue areas have experienced extensive plasticity. The visualization of the D^2_{min} shows that plasticity occurs in random regions and not in specific patterns. At the beginning of the simulation, the atoms have not deformed irreversibly, which is why there are very few white regions. As the tensile strain progresses, white and blue areas start to appear randomly, meaning that irreversible deformation has occurred.

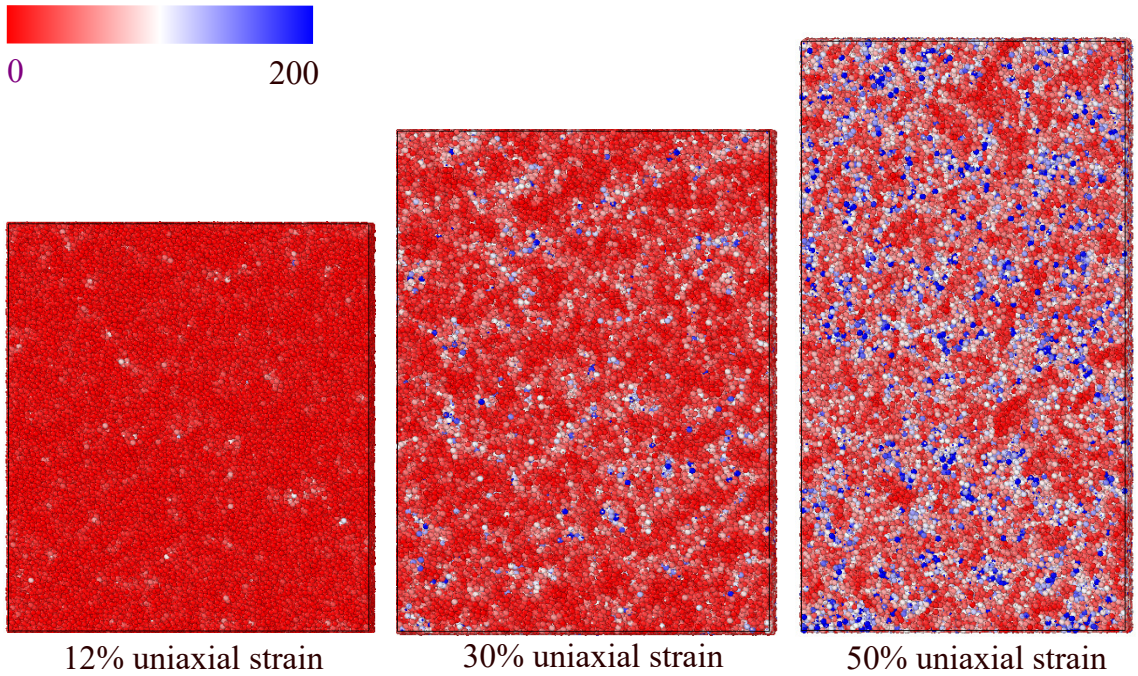

Figure 17. Cumulative non-affine squared displacement D^2_{min} in different stages of the tensile simulation. Red areas are below average D^2_{min} and blue areas are above average D^2_{min}.

In figure 18 is the cumulative distribution of D^2_{min} at 0.5 strain. It can be seen that most of the atoms have relatively low D^2_{min} values, which is reasonable considering the visualization in figure 17 showing few areas of high plasticity.

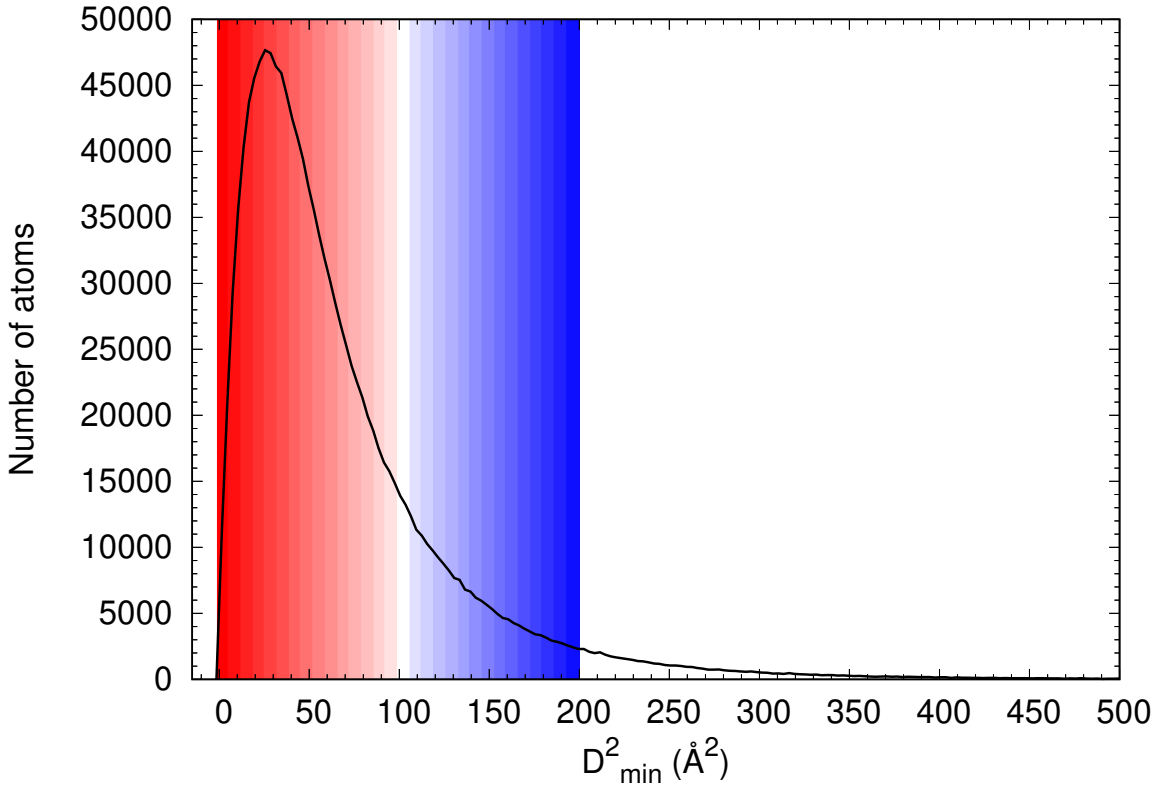

Figure 18. Cumulative non-affine squared displacement D^2_{min} at 0.5 strain. Atoms with red values are below average D^2_{min} and atoms above average D^2_{min} are blue. The white area is the average D^2_{min} at 0.5 strain, which was 111Å^2. The rest of the atoms above the average are also in blue.

5.6 Boroxol rings

The number of different membered boroxol rings was calculated throughout the entire simulation. The atoms were considered to be part of a ring if they formed a closed loop where each atom was connected to the next atom. This was done by analyzing the neighbor list of each atom and looking for atoms that were connected to each other. A ring was identified if the last atom had the initial atom as a neighboring atom. This was done for 4-, 6-, 8-, and 10-membered rings, and the results are presented in figure 19.

The average number of 4-membered rings throughout the entire simulation was approximately 6.6, and for 6-membered rings it was 117.

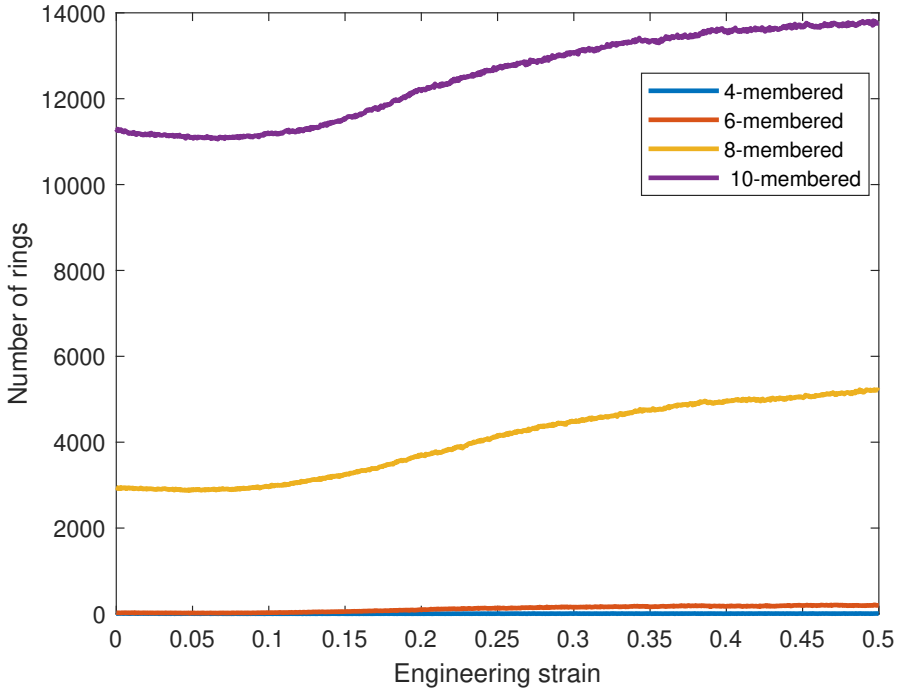

Figure 19. The number of different membered rings throughout the tensile simulation.

The number of 4-membered and 6-membered rings is low, and as the ring size grows, the number of 8-membered and 10-membered rings increases. One reason for this is the fact that an atom was allowed to belong to more than one ring. This means that a 4-membered ring and a 6-membered ring that share atoms are counted as one 10-membered ring. However, this is only the case with larger rings. Such cases are rare, because there are not many 4-membered or 6-membered rings, which means that even if they are also calculated as 10-membered rings, they will not increase the number of 10-membered rings significantly. Figure 20 illustrates a couple of these rings that share atoms. In the same figure is also an 8-membered ring and the majority of the rings were these sorts of rings. Some were more planar than others. One other possible reason for the increase in the larger rings is that as the structure deforms, the weak van der Waals bonds connecting the BO_3 units are able to deform in a way that larger rings are formed. Furthermore, bond switching might also cause the formation of larger rings because the increase in the number of rings begins where the plastic deformation starts.

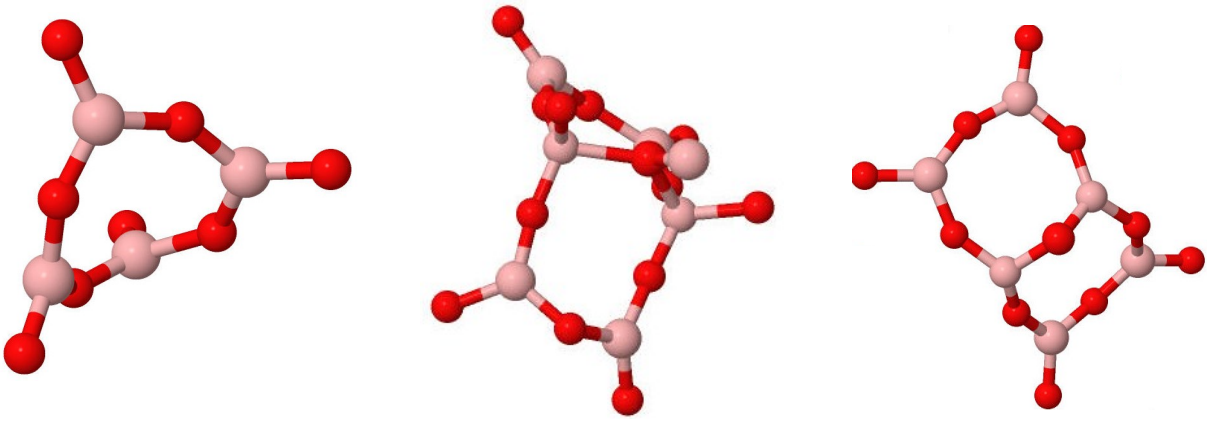

Figure 20. Different 8-membered rings found in the structure. Oxygen atoms are red and boron atoms are light pink. The ring on the left is the most common type of ring in the structure, and it is bending slightly out of the plane. The two other rings are examples of rings that share atoms.

6 Discussion

To measure the elastic deformation, Young's modulus was calculated, and it was 25.3 GPa which is quite a low value for glass. This is due to the structure of boron oxide, which consists of corner-sharing BO_3 triangles that are connected by bridging oxygens. Corner-sharing BO_3 triangles are considered to form a more fluid structure compared to tetrahedral-shaped building blocks, such as SiO_4, where they are connected at all four corners [1]. Because the fluidity is higher with triangle-shaped building blocks, it is natural that Young's modulus is low for boron oxide. In addition to the triangle-shaped building blocks, the dimensionality of boron oxide plays a part in the fluidity of the structure. Boron oxide does not have a proper three-dimensional structure since the basic building blocks are planar BO_3 triangles [3]. This means that the bonds outside the planes are fragile, and the primary bonds are only within these planes. The bonds in the third dimension can easily break, allowing for easier disruption of the structure. Therefore, Young's modulus increases as the dimensionality changes from a chain structure to a proper three-dimensional structure [3]. Furthermore, boron oxide has a low glass transition temperature (260°C), which also explains the low Young's modulus. Low glass transition temperature indicates low Young's modulus [3].

The dimensionality can also explain the low ultimate stress of boron oxide, which was approximately 2.6 GPa. Because of the low ultimate stress, boron oxide can not withstand high stress and starts to deform when relatively low stress is applied. For comparison, aluminum oxide has an ultimate stress of 7 GPa and for silica it ranges from $11 - 17$ GPa, depending on the quenching pressure [8]. For example, in silica, the proper three-dimensional structure increases viscosity, and therefore larger amounts of bonds need to be broken and reformed to increase fluidity. In boron oxide, the bonds outside of the planar structure are weak van der Waals bonds, meaning that fewer primary bonds need to be broken and reformed in order for the structure to have lower viscosity. The weaker bonds outweigh the strong bonds, which further increases the distortion of the structure [3]. Of all these three oxides, boron oxide is the most elastic and has the lowest ultimate stress. Furthermore, the higher Poisson's ratio for boron oxide (0.33) indicates that it exhibits a large elastic deformation. In contrast, Poisson's ratio for aluminum oxide is

0.297 [4].

Based on the high elasticity of boron oxide and the lack of proper three-dimensional structure, it seems that as stress is applied, the structure starts to unfold in a similar way that a crumbled paper would unfold. This could explain the high elasticity since the structure is still able to return back to the "crumbled" form. Once this is not possible, plastic deformation starts. However, specific analysis for this was not done in this thesis but it would be useful to do in the future. Especially how the bonds outside of the planar structure move and how the torsion angles change.

The planar structure in boron oxide can be easily observed in the bond angle distribution in figure 16. The bond angle distribution for O-B-O has a sharp peak only at 120°, which confirms the planar structure of boron oxide. Boron oxide is known for its strong chemical order of O-B-O bonds, which explains why there are no other peaks in the distribution and also the narrowness of the peak [24]. The planarity of the structure could be further analysed by calculating the improper torsional angles and visualizing them.

In addition, the distribution of B-O-B bond angles was also calculated. These are the bonds that connect the BO_3 building blocks and cause the bending and twisting outside of the planar structure [3]. For larger rings, the B-O-B angle is known to be over 130°, and for smaller rings, such as 6-membered, it is 120° [30]. There is a wide peak at 155° for B-O-B bond angles. This suggests the presence of larger rings that distort the planar structure. The distribution for B-O-B angles is quite wide, which makes sense considering that these angles can differ substantially within larger rings. In 6-membered rings, both B-O-B and O-B-O bond angles would be strictly 120°, resulting in a planar ring. The absence of a peak at 120° for B-O-B bonds suggests a lack of a notable number of 6-membered rings. Although experiments show a large fraction of 6-membered boroxol rings, MD simulations have not been able to produce such results [24]. The number of boroxol rings obtained from MD simulations does not have precise and consistent values in literature. On this note, the number of 6-membered rings found in this structure was low. One reason for this might be that the force field used was not accurate for this purpose. However, a larger amount of 8-membered and 10-membered rings were found. This is in agreement with the B-O-B bond angle distribution.

The plastic deformation observed in the stress-strain curve was studied by calculating the change in the coordination number throughout the tensile simulation. At the end of the tensile simulation, the vast majority of the atoms had an unchanged coordination number. This means that the atoms had to switch bonds in order to remain in their preferred

coordination and also to avoid fracture. The weaker bonds outside of the planar structure are more prone to disruption and from the figure 15 it can be seen that the fractions for 2-coordinated and 3-coordinated oxygens varied slightly more than the respective coordinates for boron atoms. The bonds that have oxygen atoms in the center are the bonds that twist the structure out of the plane. Since the weak bonds outweigh the primary bonds, it is natural that also the bond angles that have boron as a center atom start to distort, which promotes plastic deformation.

Bond switching analysis has been done for aluminum oxide by Frankberg et al.[4], where a cubic box of aluminum oxide was subjected to 50% tensile stress, and at the end around 55% of the atoms had at least one new neighboring atom, which means that bond switching occurs more in aluminum oxide compared to boron oxide. One of the reasons for this is the different structures, as aluminum oxide is considered to be almost always in a tetrahedral shape and has a proper three-dimensional structure [3]. However, according to the results of Frankberg et al. around $70 - 75\%$ of the aluminum atoms were 4-coordinated, which is less than the amount of 3-coordinated borons in boron oxide. Because aluminum atoms can have other coordination numbers, it is natural that the fraction of increased/decreased coordination numbers was higher compared to boron oxide. For aluminum oxide, at the end of the simulation around 20% of the atoms had decreased coordination number and around 18% of the atoms had increased coordination number.

Another difference is that in aluminum oxide, only approximately 10% of the atoms remained in the same coordination number and had the same neighboring atoms, which is quite different from boron oxide. In boron oxide, over half of the atoms remained in the same coordination number and had the same neighboring atoms. Still, both of them show a similar amount of plasticity. The main difference is the amount of bond switching. Boron oxide was able to deform plastically while remaining in the original coordination numbers and thus required less bond switching since the BO_3 building blocks are not easily broken. Therefore the flexible van der Waals bonds connecting the building blocks allow the deformation. Aluminum oxide requires more bond switching in order to deform plastically since the proper three-dimensional structure means that more bonds need to be broken and reformed. Moreover, the local deformation in boron oxide was not as drastic as in aluminum oxide. This can also be confirmed by comparing the non-affine squared displacements, where for aluminum oxide the average cumulative $D^2_{\text{min}} \approx 500\text{Å}^2$ at 0.5 strain [4], and for boron oxide $D^2_{\text{min}} \approx 111\text{Å}^2$ at 0.5 strain. The lower value means the the atoms had not deviated much from the original structure.

In addition, similar simulations have been done for silica. Silica has not shown plasticity to the same extent as aluminum oxide [4, 8]. As mentioned earlier, silica has a much higher ultimate stress compared to boron oxide and aluminum oxide, which are able to deform plastically without a fracture. Moreover, the activation energy for breaking a boron-oxygen bond is lower compared to silicon-oxygen bond, meaning that bond switching can not happen as easily in silica glass as in boron oxide glass, which could explain their different mechanical behavior [4, 30].

Finally, it is important to mention that MD simulations, like all computational methods, are based on assumptions. Therefore, it is good to keep this in mind when interpreting the results. Probably the biggest cause of inaccuracies in MD is the potential model used. Fortunately, the BKS potential used here has been shown to produce accurate densities and Young's modulus values that match experimental data for boron oxide [2].

7 Conclusions

The mechanical properties of boron oxide were studied with classical molecular dynamics simulations. Uniaxial tensile stress was applied to a cubic box containing 1.3 million atoms at room temperature. No fracture was observed up to 50% tensile strain, therefore boron oxide shows signs of plastic deformation. The plastic deformation occurred because of bond switching and the lack of a proper three-dimensional structure. At the end, around 44% of the atoms had at least one new neighboring atom, thus a considerable amount of bond switching had occurred. The structure of boron oxide was found to be rigid, which caused the coordination numbers to remain the same throughout the simulation even though bond switching occurred. Consequently, there was hardly any difference in the coordination numbers of 3-coordinated boron atoms and 2-coordinated oxygen atoms. The weak van der Waals bonds connecting the planar BO_3 units allowed the structure to deform plastically while remaining in the same coordination numbers.

The plastic events occurred in small regions randomly throughout the tensile simulation, increasing towards the end. However, on average, the atoms had not undergone extensive plastic deformation because they remained mostly in their original coordination numbers, and over half of the atoms even had the same neighboring atoms at the end of the simulation. These random plastic events are expected because plasticity in glasses does not occur in dislocation planes, as in crystalline solids. The plasticity observed in boron oxide falls within a similar range as in aluminum oxide, but the structural differences explain why there is less bond switching in boron oxide. Moreover, boron oxide shows greater ductility compared to silica, which is another common glass former.

The lack of a proper three-dimensional structure was found to be the reason for the surprisingly low Young's modulus, which was 25.3 GPa. Triangle-shaped building blocks allow for easier disruption of the structure and increase fluidity. Furthermore, the low ultimate stress indicates that the structure can be easily disrupted and unfolded from the original structure, and therefore experiences large elastic deformation.

Potential future simulations could include studying the tensile and compressive deformation of boron oxide nanopillars. Furthermore, investigating larger planar rings and their torsion angles could give valuable information on how the structure of boron oxide

unfolds from a "crumbled paper"-like structure to a flatter structure.

References

[1] A. K. Varshneya and J. C. Mauro. *Fundamentals of Inorganic Glasses*. Academic Press, 1993.

[2] P. Sahu, A. A. Pente, and M. D. Singh. "Molecular Dynamics Simulation of Amorphous SiO2, B2O3, Na2O–SiO2, Na2O–B2O3, and Na2O–B2O3–SiO2 Glasses with Variable Compositions and with Cs2O and SrO Dopants". In: *The Journal of Physical Chemistry B* 123 (2019), pp. 6290–6302. DOI: 10.1021/acs.jpcb.9b03026.

[3] J. E. Shelby. *Introduction to Glass Science and Technology, Second Edition*. The Royal Society of Chemistry, 2005.

[4] E. J. Frankberg et al. "Highly ductile amorphous oxide at room temperature and high strain rate". In: *Science* 366 (2019), pp. 864–869. DOI: 10.1126/science.aav1254.

[5] P. Debenedetti and F. Stillinger. "Supercooled liquids and the glass transition". In: *Nature* 410 (2001), pp. 259–267. DOI: https://doi.org/10.1038/35065704.

[6] J. B. Wachtman, W. R. Cannon, and M. J. Matthewson. *Mechanical Properties of Ceramics, Second Edition*. John Wiley Sons, Inc, 2009.

[7] J. Zhang et al. "Plastic deformation in silicon nitride ceramics via bond switching at coherent interfaces". In: *Science* 378 (2022), pp. 371–376. DOI: DOI:10.1126/science.abq7490.

[8] J. Zhang et al. "Room temperature plasticity in amorphous SiO2 and amorphous Al2O3: A computational and topological study". In: *Acta Materialia* 259 (2023). DOI: https://doi.org/10.1016/j.actamat.2023.119223.

[9] E. J. Frankberg et al. "Exceptional Microscale Plasticity in Amorphous Aluminum Oxide at Room Temperature". In: *Advanced Materials* 35 (2023). DOI: https://doi.org/10.1002/adma.202303142.

[10] M. P. Allen and D. J. Tildesley. *Computer Simulation of Liquids*. Clarendon Press, 1987.

[11] A. Pedone et al. “Interatomic potentials for oxide glasses: Past, present, and future”. In: *Journal of Non-Crystalline Solids: X* 15 (2022). DOI: https://doi.org/10.1016/j.nocx.2022.100115.

[12] A. R. Leach. *Molecular Modelling: Principles and Applications (2nd edition)*. Elsevier Academic Press, 2001.

[13] F. Jensen. *Introduction to Computational Chemistry*. Wiley, 2007.

[14] J.-P. Hansen and I. McDonald. *Theory of Simple Liquids (3rd Edition)*. Pearson Education, 2006.

[15] M. González. “Force fields and molecular dynamics simulations”. In: *Collection SFN* 12 (2011), pp. 169–200. DOI: https://doi.org/10.1051/sfn/201112009.

[16] D. Frenkel and B. Smit. *Understanding Molecular Simulation : From Algorithms to Applications*. Elsevier Science Technology, 2001.

[17] H. Kumar and P. K. Maiti. “Introduction to Molecular Dynamics Simulation”. In: *Computational Statistical Physics: Lecture Notes, Guwahati SERC School*. Hindustan Book Agency, 2011, pp. 161–197. DOI: 10.1007/978-93-86279-50-7_6.

[18] W. G. Hoover. “Canonical dynamics: Equilibrium phase-space distributions”. In: *Physical Review A* 31 (1985), pp. 1695–1697. DOI: 10.1103/PhysRevA.31.1695.

[19] W. G. Hoover. “Nosé-Hoover Nonequilibrium Dynamicsand Statistical Mechanics”. In: *Molecular Simulation* 33 (2009), pp. 13–19. DOI: https://doi.org/10.1080/08927020601059869.

[20] L. Montelli and D. P. Tielemn. “Force fields for classical molecular dynamics”. In: *Methods Mol Biol.* 924 (2013), pp. 197–213. DOI: 10.1007/978-1-62703-017-5_8.

[21] B. W. H. van Beest, G. J. Kramer, and R. A. van Santen. “Force fields for silicas and aluminophosphates based on ab initio calculations”. In: *Phys. Rev. Lett.* 64 (16 1990), pp. 1955–1958. DOI: 10.1103/PhysRevLett.64.1955.

[22] D. C. Rapaport. *The Art of Molecular Dynamics Simulation*. Cambridge University Press, 2004.

[23] W. H. Zachariasen. “The atomic arrangement in glass”. In: *J. Am. Chem. Soc.* 54 (1934), pp. 3841–3851. DOI: https://doi.org/10.1021/ja01349a006.

[24] R. A. Barrio et al. “Evaluation of the concentration of boroxol rings in vitreous B2O3 by the stochastic matrix method”. In: *Journal of Physics: Condensed Matter* 9 (1997), pp. 9219–92347. DOI: DOI:10.1088/0953-8984/9/43/008.

[25] N. E. Dowling. *Mechanical Behavior of Materials*. Pearson Education Limited, 2013.

[26] W. F. Hosford. *Fundamentals of Engineering Plasticity*. Cambridge University Press, 2013.

[27] A. P. Thompson et al. “LAMMPS - a flexible simulation tool for particle-based materials modeling at the atomic, meso, and continuum scales”. In: *Comp. Phys. Comm.* 271 (2022), p. 108171. DOI: 10.1016/j.cpc.2021.108171.

[28] A. Stukowski. “Visualization and analysis of atomistic simulation data with OVITO–the Open Visualization Tool”. In: *Modelling and Simulation in Materials Science and Engineering* 18 (2010). DOI: 10.1088/0965-0393/18/1/015012.

[29] M. L. Falk and J. S. Langer. “Dynamics of viscoplastic deformation in amorphous solids”. In: *Physical review E* 57 (1998), pp. 7192–7205. DOI: 10.1103/PhysRevE.57.7192.

[30] A. C. Wright and G. Dalba. “Borate Versus Silicate Glasses: Why Are They So Different?” In: *Physics and Chemistry of Glasses - European Journal of Glass Science and Technology Part B* 51 (2010), pp. 233–265.

A Radial distribution function 10 Å

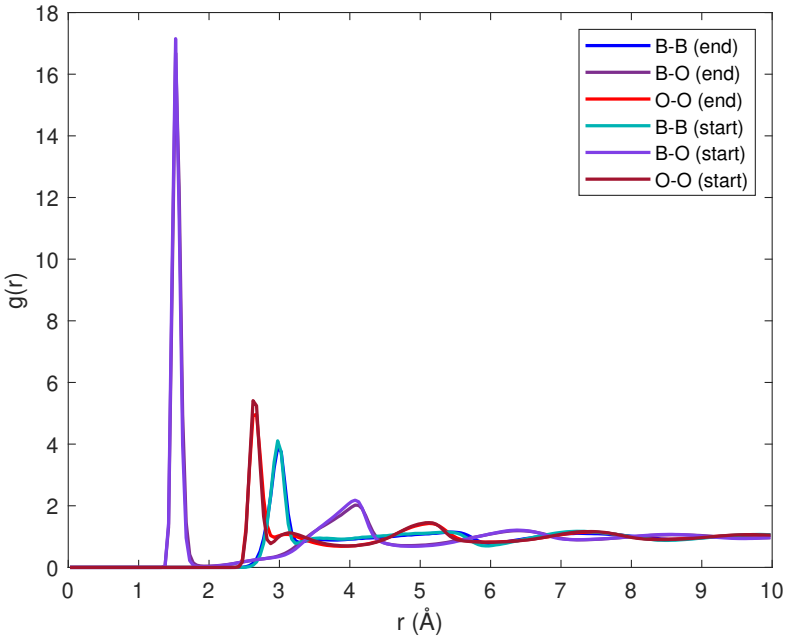

Figure 21. Radial distribution up to 10 Å.